IMAGING AND ANALYSIS OF LARVAL ZEBRAFISH GUT MOTILITY,

AND AUTOMATED TOOLS FOR 3D MICROSCOPY

by

RYAN PATRICK BAKER

A DISSERTATION

Presented to the Department of Physics
and the Graduate School of the University of Oregon
in partial fulfillment of the requirements
for the degree of
Doctor of Philosophy

September 2017

DISSERTATION APPROVAL PAGE

Student: Ryan Patrick Baker

Title: Imaging and Analysis of Larval Zebrafish Gut Motility, and Automated Tools for 3D Microscopy

This dissertation has been accepted and approved in partial fulfillment of the requirements for the Doctor of Philosophy degree in the Department of Physics by:

Eric Corwin	Chairperson
Raghuveer Parthasarathy	Advisor
Stephanie Majewski	Core Member
Judith Eisen	Institutional Representative

and

Sara D. Hodges	Interim Vice Provost and Dean of the Graduate School

Original approval signatures are on file with the University of Oregon Graduate School.

Degree awarded September 2017

DISSERTATION ABSTRACT

Ryan Patrick Baker

Doctor of Philosophy

Department of Physics

September 2017

Title: Imaging and Analysis of Larval Zebrafish Gut Motility, and Automated Tools for 3D Microscopy

Nearly all individual members of the animal kingdom have gastrointestinal tracts which feature unique cellular compositions, geometries, and temporal dynamics. These guts are distinct enough from one another, even across siblings or even across the same individual at different points in space and time, that defining meaningful scientific representations of those features is difficult. Studying these guts is also innately challenging as it requires accessing to the insides of the enclosed 3D volumes.

The work presented here describes tools and methodologies designed to address these difficulties. To investigate gut motility, we constructed a combined light sheet fluorescence and differential interference contrast microscope to obtain videos of larval zebrafish (*Danio rerio*) gut motility and to obtain 3D information about nearby fluorescently tagged cells. Using advanced computer vision algorithms, we quantified aspects of zebrafish gut motility which have never before been characterized, then used that information to identify the effects of different genetic, chemical, and physiological states of zebrafish gut motility. Finally, we designed and constructed an instrument for automating 3D microscopy for future studies.

This dissertation includes previously published and unpublished co-authored material.

CURRICULUM VITAE

NAME OF AUTHOR: Ryan Patrick Baker

GRADUATE AND UNDERGRADUATE SCHOOLS ATTENDED:

University of Oregon, Eugene
University of Nevada, Reno

DEGREES AWARDED:

Doctor of Philosophy, Physics, 2017, University of Oregon
Bachelor of Science, Physics, 2011, University of Nevada, Reno

AREAS OF SPECIAL INTEREST:

Scientific Programming.
Quantitative Image Analysis.
Fluorescence and Phase Microscope Design.
High-Throughput Automated Imaging.

PROFESSIONAL EXPERIENCE:

Research Assistant, Parthasarathy Lab, University of Oregon, 2012-2017

Research Assistant, Weinstein Lab, University of Nevada, Reno, 2010-2011

GRANTS, AWARDS, AND HONORS:

Technology Entrepreneurship Program Fellow, University of Oregon, 2015

PUBLICATIONS:

R. P. Baker, J. Ganz, M. K. Hamilton, E. Melancon, P. Diba, J. S. Eisen, and
R. Parthasarathy, (2017). *bioRxiv*.

Wiles, T. J., Jemielita, M., Baker, Ryan P., Schlomann, B. H., Logan, S. L., Ganz, J., Parthasarathy, R. (2016). *PLoS Biology*, 14(7), 1–24. https://doi.org/10.1371/journal.pbio.1002517

Baker, Ryan P., Taormina, M. J., Jemielita, M., & Parthasarathy, R. (2015). *Journal of Microscopy*, 258(2). https://doi.org/10.1111/jmi.12220

Li, T., Baker, Ryan P., & Weinstein, J. D. (2012). *Journal of the Optical Society of America B*, 29(10), 2848–2851.

ACKNOWLEDGMENTS

TABLE OF CONTENTS

Chapter   Page

LIST OF FIGURES

CHAPTER I

INTRODUCTION

Overview and Motivation

The proper transit of nutrients through the gastrointestinal tract of an animal requires the coordination of, among other things, smooth muscle cells, pacemaker cells, neurons, and electrical signals [1]. As one might expect, small perturbations to any one of these cells or their functions in space or time can often have dire consequences for the health of an animal [2, 3]. Studying these issues, however, requires overcoming a simple yet important geometry problem: studying the inside of any volume requires going through that its surface.

This problem isn't trivial in the case of gastroenterology research. Many tools developed for measuring gut activity require invasive or destructive procedures, from a rectally administered colonic catheter in sedated humans [4] to the euthanasia of guinea pigs and subsequent excision of their guts [5]. And for those scenarios in which the animals are not euthanized, it's known that animals experiencing a variety of stressors undergo changes in bowel movements [6], meaning any measurements made with invasive procedures might alter the motility itself. In addition, such probes are often difficult to use, resulting in challenges in interpreting results from different sources [7] and are often limited to very specific use scenarios [4, 7]. For instance, colonic catheters require patients to clear their bowels and not eat for 24 hours before the catheter is administered, and the administration process requires sedating the patient and subsequently waking them to

measure gut activity while they lay still, in a lab, for extended periods of time (several hours, in some cases) [4].

Accurate quantitative representations of gut motility are further complicated by the complexity of the system. Parameterizing large collections of multicellular masses which move in space and time often requires projecting that complex motion into a small set of easily measured parameters. While this has been fruitful for measured parameters such as the frequency of gut movements or the wave speed of motility events as they travel along a gut [5, 6, 8-12], there are likely other qualities of gut motility which are altered under various chemical, physiological, or genetic perturbations which are not captured using current techniques.

One route commonly taken to avoid these complications is to optically image the gut motility of small, nearly transparent host organisms such as zebrafish *(Danio rerio)* [8-11, 13, 14]. This has the additional advantages that zebrafish reproduce quickly and produce large clutches, providing better statistics than other vertebrate model organisms. In addition, there are a variety of transgenic lines available, providing researchers a set of controls for altering some aspects of the model organism. Zebrafish are also vertebrates, making research results concerning the organism's health more likely to be relevant to human health.

The goal of this thesis is to disseminate tools and techniques I've developed for combatting all of the previously mentioned issues, using the zebrafish as a model organism. Chapter II will focus on the design and construction of a combined fluorescent and phase contrast microscope which has allowed me to obtain *in vivo* measurements of the gut

activity of live zebrafish with great optical clarity and without destructive alteration to the organism. It contains published coauthored material with contributions from Michael J. Taormina, Matthew Jemielita, and Raghuveer Parthasarathy. Chapter III will describe in detail the analysis method I've developed for characterizing and quantifying gut motility, as well as the experiments performed to measure and compare various gut states. These states include chemical perturbations, fed and unfed states, and genetic alterations to zebrafish gut innervation. It contains published coauthored material with contributions from Julia Ganz, Kristi Hamilton, Ellie Melancon, Parham Diba, Judith Eisen, and Raghuveer Parthasarathy. Chapter IV will then describe the design and construction of a high-throughput device for automating the imaging of our model organism. It contains unpublished material which will be coauthored by Savannah Logan, Christopher Dudley, Michael Taormina, Teddy Hay, and Raghuveer Parthasarathy. Finally, Chapter V will provide conclusions regarding this work and ideas for future expansion.

CHAPTER II

A COMBINED FLUORESCENCE AND PHASE MICROSCOPE

This chapter has been partly adapted from previously published material coauthored with Michael J. Taormina, Matthew Jemielita, and Raghuveer Parthasarathy. This work was published in volume 258 of the Journal of Microscopy in 2015 under the name "A combined light sheet fluorescence and differential interference contrast microscope for live imaging of multicellular specimens" [18]. Michael Taormina and Matthew Jemielita built the original fluorescence microscope. I designed and built the additional phase microscope and integrated it into the original fluorescence microscope. Raghuveer Parthasarathy was the principle investigator for this work.

Motivation

Combinations of different microscope technologies have been around for a long time. Surprisingly, however, at the start of my research there had not been a single microscope design that used both Light Sheet Fluorescence Microscopy (LSFM) and Differential Interference Contrast Microscopy (DICM). The integration of the two techniques seemed like a perfect combination as it would provide two complementary imaging modes that would work well with zebrafish. In particular, LSFM provides three-dimensional imaging of fluorescently labelled components of multicellular systems with high speed, large fields of view, and with low phototoxicity. In contrast, DICM reveals the unlabelled neighborhood of tissues, organs, and other structures (even transparent

structures, as is the case with larval zebrafish) with high contrast and with inherent optical sectioning. In terms of what would eventually become the subject matter of this thesis, this combination was necessary, for most of the data presented in this dissertation has come from the DICM and a great deal of the zebrafish imaging infrastructure at the time had been designed around the unique LSFM geometries. This combination has also been valuable for research not presented in this thesis and has been used by others for studying host-microbiome interactions, killing mechanisms in bacteria while inside a host, and other gut motility research, all performed by colleagues here at the University of Oregon.

At the start of this project, the LSFM component of the combined microscope had already been designed and built by Michael Taormina and Matthew Jemielita, two previous graduate students in the Parthasarathy lab. It is the subject matter of part of their theses and has also been published [19]. Therefore, a comprehensive overview of the LSFM design and implementation can be found there. The DICM portion of the microscope, however, is detailed more explicitly below, taken from material we published on the subject [18].

Introduction

Embryonic and larval development occurs via the coordinated interactions of large numbers of cells. Imaging developmental processes therefore presents significant technical demands, calling for methods that can span organs, tissues, or even whole organisms with sufficient resolution in three dimensions to track individual cells, sufficient speed to capture snapshots unblurred by cellar motions, and sufficiently low phototoxicity to allow imaging for the long durations of morphogenetic processes. In recent years, the technique of light
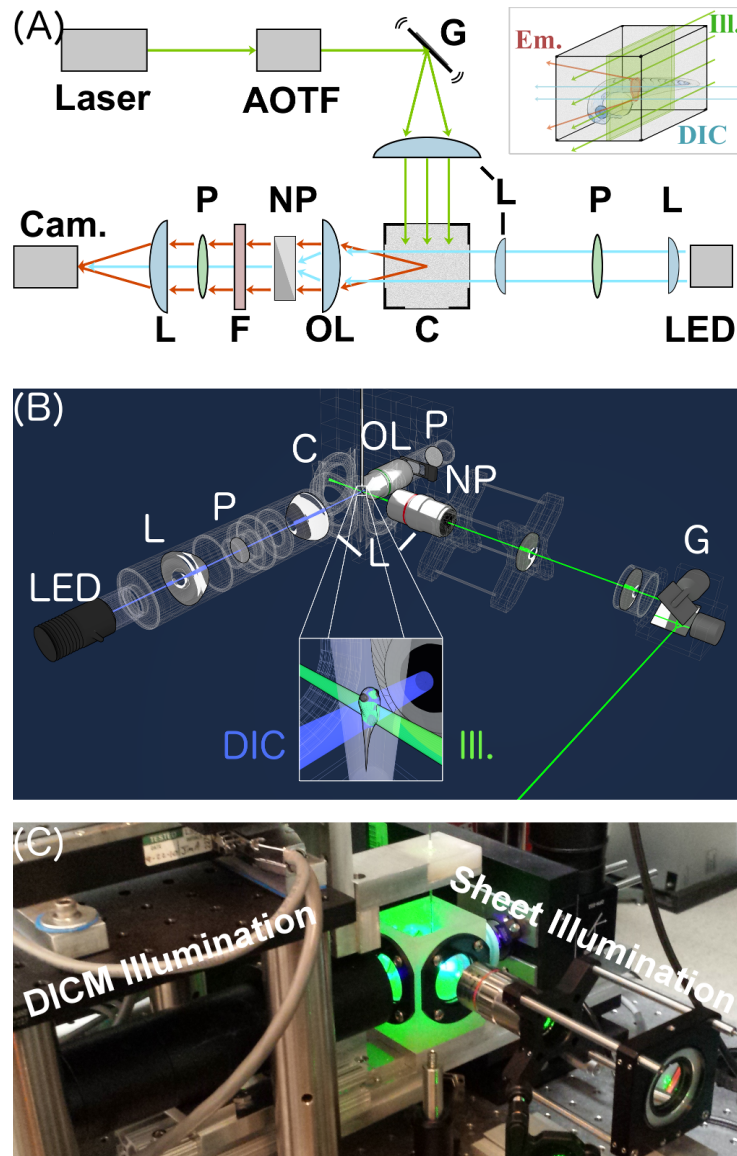
Figure 1. A combined light sheet fluorescence and differential interference contrast microscope. (A) Block Schematic. G=Galvometer, L=Lens, P=Polarizer, C=Chamber, OL=Objective Lens, NP=Nomarski Prism, F=Filter Wheel, Cam=Camera, LED=Light Emitting Diode, AOTF=Acousto-Optical Tunable Filter. (B) 3D Model of the physical setup with components labelled. (C) Physical Setup.

sheet fluorescence microscopy (LSFM), also known as selective plane illumination microscopy (SPIM), has emerged as a powerful approach for three-dimensional live

imaging, satisfying the above requirements [20-27]. In brief, LSFM involves illumination

of a specimen with a thin sheet of fluorescence excitation light, the emission from which is

imaged onto a camera via a perpendicular lens (Fig. 1). Scanning the specimen in only one

dimension, perpendicular to the sheet, rapidly generates a three dimensional image.

Moreover, in stark contrast to, for example, confocal microscopy, every part of the

specimen that is illuminated is imaged, leading to very low levels of photobleaching and

phototoxicity [19, 20].

Several research groups have extended the imaging capabilities of LSFM through,

for example, the integration of structured illumination [28], localization-based

superresolution [29], stimulated emission depletion [30], and multiphoton excitation [31]. It

is notable that all of these methods, while certainly useful, rely on fluorescence, as does

LSFM itself. Often in biological imaging, fluorescently labeled cells or cellular structures

of interest, by construction, make up a subset of all the cells in their neighborhood. One can

image, for example, migrating sensory cells [27], firing neurons [26], or gut microbes [32],

but the function and behavior of these and other specific cell types can be modulated by the

cells and biomaterials of their local neighborhood. In a complex multicellular organism,

however, simple brightfield imaging is insufficient to make sense of the unlabeled cellular

environment.

Differential interference contrast microscopy (DICM) has a long history as a

powerful imaging method for generating optical contrast and sectioning using transmitted

light [33, 34]. In DICM, light from slightly spatially separated paths is recombined such

that the resulting intensity is a measure of the difference in optical path length. Roughly, the

image intensity is a measure of the gradient of the index of refraction in the focal plane, and therefore provides contrast to edges in transparent structures like collections of cells.

While DICM is a well-established technique, it has never been combined with light sheet fluorescence imaging (In contrast, several groups have integrated DICM with confocal imaging, e.g. [35, 36]). We show here that combining DICM and LSFM is straightforward to implement, and we provide examples illustrating that, as claimed above, differential contrast imaging provides useful tissue-level context for light sheet fluorescence microscopy. Our examples focus mainly on imaging of the digestive tract of larval zebrafish, in which the existence of multiple tissue types and multiple species, fish and microbes, provide a challenging imaging environment.

Experimental Setup

Various designs for LSFM have been developed in recent years [21, 23, 24, 25], all of which involve the illumination of a specimen with a thin sheet of fluorescence excitation light and the detection of emission along an axis perpendicular to the sheet. The light sheet fluorescence design aspects of our home-built instrument (Fig. 1) closely follow the designs of Keller et al. (2008) [20] and are described in detail in Reference Taormina et al., 2012 [32]. In brief: One of several laser lines (Coherent, SantaClara, CA, USA, Sapphire 561 and 488) is selected with an acousto-optical tunable filter (Crystal Technology, Palo Alto, CA, USA, AODS20160) and swept by a rapidly scanning galvanometer mirror (frequency 500Hz, Cambridge Technology, Bedford, MA, USA 6210H). A telecentric f-theta lens transforms the angular sweep into a translational sweep, which then passes

through a tube lens and objective lens (Mitutoyo Aurora, IL, USA, M Plan APO, 5x) to reach the specimen. Emission light is filtered with a bandpass filter (Chroma Technology Bellows Falls, VT, USA) and magnified by an objective lens (Zeiss Oberkochen, Germany DICM M Plan Apochromat, 40x/1.0) and tube lens onto a scientific CMOS camera (Cooke, Kelheim, Germany, pco.edge). Typical exposure times for each image plane are 10-100 ms, which are long compared to the sweep frequency of the light sheet. Our set-up is illustrated in Figure 1.

DICM is a method for transforming spatial variation in the index of refraction or thickness of a sample into contrast in an image. DICM has been a well-established imaging technique for decades, and detailed treatments of its optics exist in the literature [33, 37, 38, 39]. In order to make this report self-contained, we provide a short explanation of this method. Consider polarized light incident on a sample. In the infinity space of the imaging light path, a Nomarski prism deflects light of orthogonal polarizations, chosen to be oriented at 45 degrees relative to the incident polarization axis, along different directions. This angular shear of the differently polarized transmitted rays is transformed by the microscope's tube lens into a lateral separation. The light also passes through a polarizer (known as the analyzer) oriented at 90 degrees relative to the illumination polarization, before being detected, typically by a camera. Note that light from a single point in the object plane reaches two points at the camera plane, one corresponding to each polarization generated the Nomarski prism. Equivalently, light from two spatially separated points in the object plane will reach the same point in the camera plane, and the analyzer orientation ensures that their interference will depend on the relative path length difference of the two

paths. DICM therefore effectively computes a directional derivative of the optical path length of a specimen and displays the result as image contrast.

The argument above is valid if the light used to illuminate the sample is spatially coherent at the object plane, so that there is a well-defined phase relationship between separated points. It is therefore critical to maintain coherence over at least the shear distance. A standard approach to achieving this is to add a Nomarski prism to the beam path between the condenser lens, and the specimen. By separating components of the polarization of the illumination light by exactly the desired shear distance in the object plane, one guarantees that any phase difference acquired by the components was obtained via a difference in optical path length through the sample (assuming temporal coherence). Another approach is to use a light source that is coherent over distances greater than or equal to the shear distance. It has been well known for decades that LEDs have limited spatial coherence, and many researchers have made use of this property for microscopy. Bormuth et al. (2007) [40] specifically described and characterized the use of LEDs for DICM illumination, and we adopt their approach. Mehta and Sheppard (2008) [38] described in detail the optics of DICM with a single prism. One could also use a highly coherent source, such as a laser, though this has the practical disadvantage of easily generating speckle in images.

Our DICM set-up uses a 447 nm LED as an illumination source (Quadica Developments Luxeon Star Brantford, Ontario, Canada) and uses only one Nomarski prism (Zeiss), as explained above (Fig. 1). The microscope is designed such that the same detection optics are used for light sheet fluorescence and DICM imaging. The addition of a
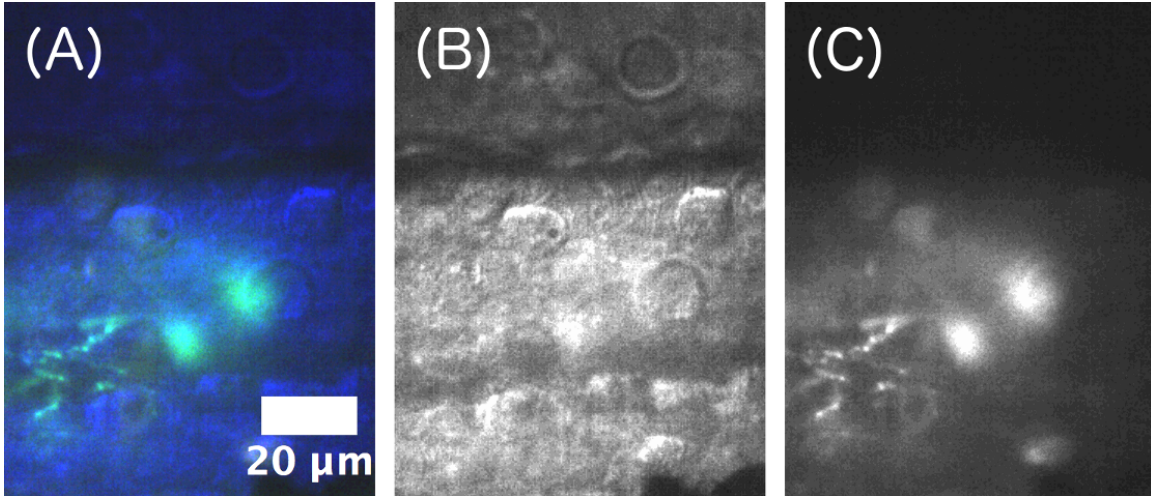
Figure 2. (A) Image of a zebrafish gut, taken while DICM and LSFM were used simultaneously. The image of the unlabelled gut was acquired with a blue LED and the neurons expressing GFP emit green light. (B) Blue color channel of the RGB image in (A). (C) Green color channel of the RGB image in (A).

Nomarski prism to the beam path does not introduce noticeable optical aberrations to the imaging of the incoherent fluorescent emission (quantified below). Because the Nomarski prism and polarizer pairs are located in the infinity space separating the objective and tube lens, insertion and removal of these optical elements is straightforward.Wavelength filtering or control of the LED power supply enable switching between fluorescence and DICM imaging. In addition, since DICM and LSFM can be done at different wavelengths, one can simultaneously acquire both DICM and LSFM images. We demonstrate this (Fig. 2) by using a color camera (Thorlabs, Newton, NJ, USA, Moticam 2000), but one could also spatially split the colors and image onto two separate cameras, or onto different regions of a single camera sensor. Notably, the combined LSFM and DICM instrument (Fig. 1) can incorporate various modifications to light sheet microscopy, such as structured
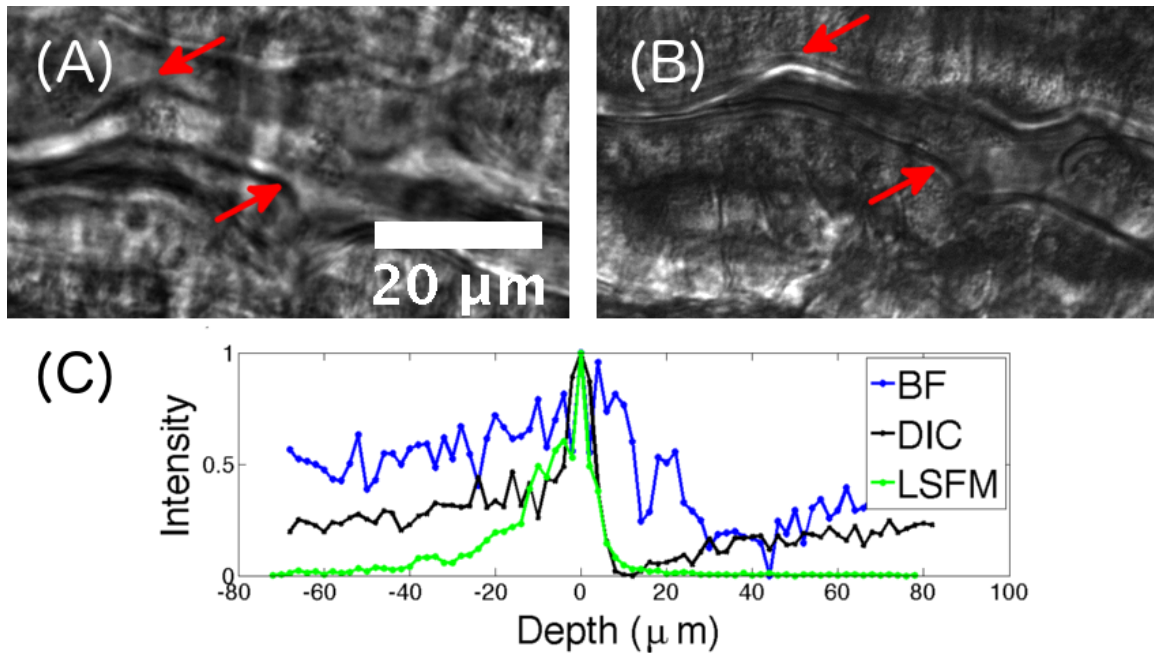
Figure 3. Characterization of various imaging techniques. (A) Brightfield and (B) DICM images of the same region of the intestine of a 7 days post-fertilization larval zebrafish. In the DICM image, features such as the gut edge (arrows) are clearly evident. (C) Pixel intensity, normalized to a peak value of 1, as a function of depth relative to the focal plane from images of a fluorescent polystyrene microsphere embedded in agar imaged with BF (brightfield), DICM and LSFM, providing a measure of the depth of focus, and optical sectioning ability, of each method.

illumination and multiphoton excitation, as noted above, without requiring redesign or alteration of the DICM optics. All experiments performed with zebrafish were done according to protocols approved by the University of Oregon Institutional Animal Care and Use Committee. The ages of all imaged zebrafish were between 5 and 7 days post-fertilization.
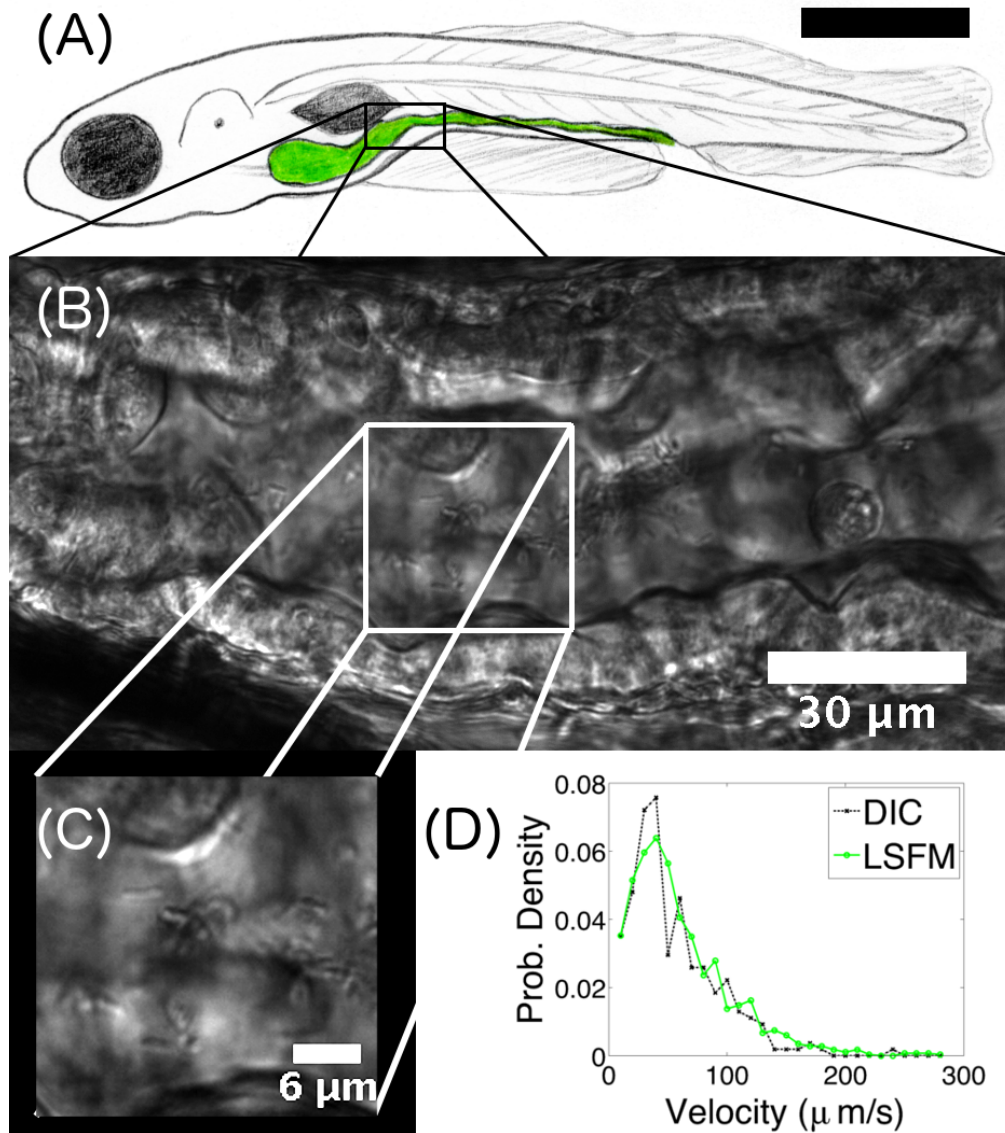
Figure 4. (A) Schematic illustration of a larval zebrafish, with the intestine highlighted in green. The scale bar is approximately 0.5 mm. (B) DICM image of a section of the intestine of a 6 days postfertilization zebrafish. The gut boundaries are clearly evident. (C) Part of the image in (B), showing individual rod-like Vibrio cholerae bacteria. (D) Velocity distribution of Vibrio cholerae in the gut, obtained from either LSFM or DICM imaging.

Results

We constructed an integrated DICM/LSFM microscope to augment information on the positions and dynamics of fluorescent cells in live specimens, especially embryonic and larval zebrafish, with information about the local environment. Zebrafish are a popular and important model organism due to their physiological similarity with other vertebrates, their fecundity, their amenability to genetic manipulation, and their transparency at young ages [41, 42]. Like all vertebrates, however, they are composed of many types of tissues, organs and extracellular materials, often making simple brightfield imaging of specimens confusing or uninformative.We provide examples of the utility of our instrument focusing especially on the larval zebrafish gut, both because of its importance as a model for studying bacteria-host interactions in vertebrates [32, 43, 44, 45] and because its complexity highlights the utility of DICM imaging. We first show brightfield and DICM images of a region of the gut (Figs. 3A,B). In the DICM image, important features such as the gut boundary and individual cells are evident.

The interferometric nature of DICM also generates well-known optical sectioning, as only a thin region around the focal plane contributes coherently to image formation. To compare the depth of field of fluorescence, brightfield, and DICM imaging we captured images of 100 nm diameter fluorescent microspheres (Life Technologies, Grand Island, NY, 488nm FlouSpheres), immobilized in agar, at a series of depths along the detection optical axis. We determined the central pixel of a bead from the in-focus two-dimensional image, and examined the intensity of this pixel as a function of image depth plotted in

Figure 3C for a single bead. The fluorescence intensity of the microsphere decays to half its maximal value within approximately 10 μm from the focal plane. This width is largely determined by the excitation sheet thickness, which can be tuned via the illumination optics and which determines the Rayleigh length of the illuminating beam. Although we are capable of achieving a near diffraction limited beam waist with our set-up, the corresponding Rayleigh length associated with this width would be much smaller than the field of view we wish to image, specifically large sections of the larval zebrafish gut. We therefore use a beam waist of roughly 10 μm, which gives a uniform sheet thickness over a roughly 500 μm extent. For different applications, different beam waists and Rayleigh lengths will be optimal. The DICM intensity of the microsphere exhibits a characteristic bright and dark pattern relative to the background, with a sharpness similar to that of the fluorescence trace, indicating section capabilities well-matched to integration with LSFM. The brightfield image is noisy, has low contrast, and its peak decays over a depth of approximately 30 μm, considerably larger than the DICM or LSFM traces.

Figure 4 shows an example of the quantitative information that can be derived from DICM imaging of the zebrafish digestive tract. Gut bacteria (Vibrio cholerae, introduced into an initially microbe-free fish (Milligan-Myhre et al., 2011) [46] are evident (Figs. 4B,C). Not only can we distinguish individual bacteria (Fig. 4C), we can also extract quantitative information about their motility. Figure 4(D) shows velocity distributions of gut bacteria obtained by the two different imaging modes of our microscope. The green curve was obtained from LSFM images of V. Cholerae expressing green fluorescent protein. The black curve was obtained from DICM images taken shortly after the LSFM
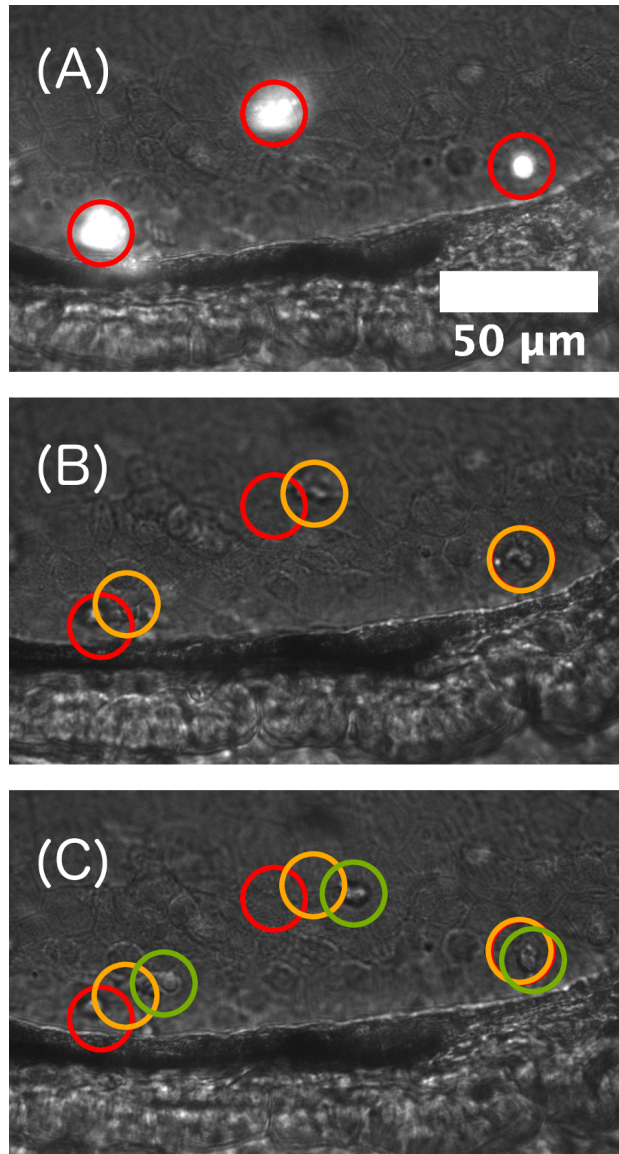
Figure 5. Motile immune cells. (A) Simultaneous DICM and LSFM image of fluorescent neutrophils (transgenic mpo:GFP) in a 5 days postfertilization larval zebrafish. (B, C) DICM images at times 185 s and 380 s before the image of panel (A), showing neutrophil motility.

images of the same region of the same fish. In both cases, bacteria were tracked using custom software that localizes bright spots in images [47]. For DICM, images were spatially and temporally filtered to extract nonstationary signals with the size characteristic
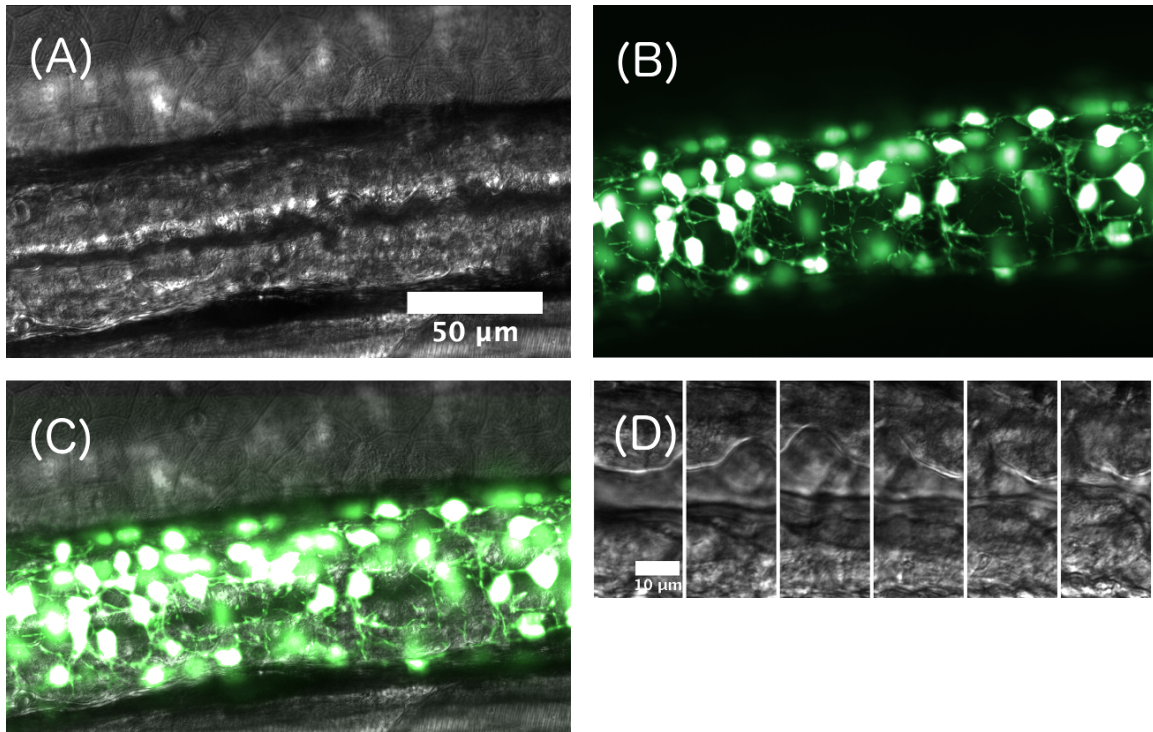
Figure 6. (A) DICM image of a 5 days postfertilization larval zebrafish gut. (B) False-color maximum intensity projection of a three dimensional LSFM image of enteric neurons. (C) Overlay of the DICM and LSFM images. Image contrast has been enhanced for clarity. (D) A time series of DICM images, separated by 1 s, showing a peristaltic wave of gut motion. Scale bar: 10 μm.

of bacteria, mean- subtracted, and smoothed to generate processed images with bright features on dark backgrounds that could then be tracked. The velocity distributions are essentially identical to one another. The mean velocities from DICM- and LSFM-derived trajectories are 55 and 60 μs−1, respectively, consistent with expected in vitro values for these microbes [48].

DICM can be used to monitor particular eukaryotic cell types or behaviors. To demonstrate this in a live animal, we show LSFM and DICM images of neutrophils, highly

motile immune cells, imaged with both DICM and LSFM in a transgenic fish (MPO:GFP) in which green fluorescent protein expression is driven by a neutrophil-specific promoter [49]. DICM images in Figure 5 show the motion of particular individual cells over 6 min, and LSFM images indicate that these cells are, in fact, neutrophils. The use of DICM to follow specific cells should be especially useful in cases in which LSFM is devoted to imaging other, different cells. Specific fluorescent transgenic animals are often unavailable or difficult to construct, and the combination of DICM and LSFM expands the set of cell types that can be examined in one experiment.

Another example of the utility of combined DICM and LSFM is provided in Figure 6, which shows a DICM image of the gut and LSFM images of enteric neurons (transgenic phox2b:GFP) that line the gut and coordinate peristaltic motions [10, 11, 13]. With the two imaging modes, the dynamics of peristalsis can be correlated with the location and the connectivity of the enteric neural network relative to the gut boundary, enabling previously inaccessible quantitative studies of the control of gut motility.

Conclusion

Three-dimensional imaging in live specimens presents many technical challenges due to its demands of large fields of view, high speeds relative to timescales of cellular motion, and low phototoxicity. We have shown that the integration of LSFM and DICM is a valuable methodology for live imaging, as it combines the specificity of fluorescence-based three-dimensional microscopy with the contextual information of DICM. The appeal of the speed and light efficiency of LSFM relative to, for example confocal microscopy for

live imaging is increasingly well appreciated [19, 21, 27, 31], and its straightforward integration with DICM should motivate even more applications to optically and biologically heterogeneous systems such as three-dimensional cell cultures, developing organs and tissues, and whole animals.

It is worth noting that part of the appeal of adding DICM to LSFM stems from the difficulty and laboriousness of creating fluorescent transgenic organisms, even with modern molecular methods. Being able to use DICM to quantify the motility of bacteria (Fig. 4D) or neutrophils (Fig. 5) - each of which provide information on chemotaxis and other response behaviors in a wide variety of contexts - frees fluorescence channels to be used for other cell types. In principle, one can create a wide range of multicolored fluorescent reporters. In practice, however, the labour of designing new fluorescent microbes or animals is significant - for bacteria, it typically involves engineering appropriate plasmids, controlling the cloning, insertion, and expression of new genes, and tedious assessments of insertion and viability, which typically take weeks to implement in new species, not always successfully. The creation of transgenic zebrafish is even more labor and time intensive. Therefore, the combination of high contrast fluorescence-based and nonfluorescent imaging modes is useful for circumventing these challenges. Integrating DICM with LSFM in particular combines two imaging methods that are ideally suited to the visualization of complex multicellular systems.

The next chapter contains experimental results obtained with the optical setup discussed in this chapter. In particular, it investigates gut motility (obtained with the DICM component of this microscope; Fig. 6D) prepared in various physiological states.

CHAPTER III

QUANTITATIVE GUT MOTILITY ANALYSIS

This chapter has been partly adapted from previously published material coauthored with Julia Ganz, Kristi Hamilton, Ellie Melancon, Parham Diba, Judith Eisen, and Raghuveer Parthasarathy. This work was published in the preprint server bioRxiv in 2017 under the name "Image velocimetry and spectral analysis enable quantitative characterization of larval zebrafish gut motility" [50]. Julia Ganz designed the initial experiments, performed some imaging, and wrote part of the manuscript. Kristi Hamilton designed another experiment and also performed some imaging and analysis. Ellie Melancon and Parham Diba prepared and maintained biological samples. I designed experiments, performed imaging, designed and wrote imaging analysis software, performed analysis, and wrote part of the manuscript. Raghuveer Parthasarathy and Judith Eisen were the principle investigators for this work.

Gut Motility Review

Proper gut motility results from the interactions between several cell types, such as muscle cells, pacemaker cells, and neurons. Most mammalian guts consist of, in addition to many other cell types, smooth muscles. These are muscles whose motile behavior is the result of electrical excitation [1, 15]. Smooth muscles are electrically coupled with a specific type of pacemaker cell known as the Interstitial Cell of Cajal (ICC). ICCs provide the smooth muscles with a continuous, location dependent rhythm known as a slow wave, a

coordinated contraction which is periodic and which has low amplitude [1-4, 8-11, 13, 15]. Slow waves are, surprisingly, capable of responding to cellular forces and pressure independently of the the system of neurons which innervate the gut [known as the Enteric Nervous System (ENS)] [1]. This fact raises an important question: if waves are generated and sustained without the ENS, and if the gut can respond to changes in gut content, what role does the ENS have in shaping gut motility? While it is known that reduced enteric neuron proliferation in the gut leads to potentially fatal health issues (for instance, Hirschsprung disease; HSCR) [2, 14] it is also known that, at least in zebrafish, the absence of the ENS does not necessarily prevent gut motility waves from occurring nor from even being coordinated (although these waves are repeatedly abnormal) [14].

Of course, motility patterns in the gut are not perfectly stereotyped. For instance, it is hypothesized that the ENS may also be capable of altering the force of peristaltic action in response to different sizes of luminal content (e.g., food) [1]. There are also different gut motility modes, such as mixing, which vary depending on various factors, such as food content or the presence of hormones [1, 4, 11, 16]. So while pacemaker cells and responses to pressure are sufficient for understanding basic motility waves, they are not sufficient for understanding all non-stereotyped gut motility patterns or for understanding why HSCR patients experience loss of colonic motility.

There are also a few known excitatory and inhibitory neurotransmitters which are necessary for proper motility and which act to communicate between the ENS and other cell types. In particular, one study showed that the addition of Acetylcholine (ACh), a principle excitatory transmitter for neurons [16, 17] was sufficient for recovering from gut

motility dysfunction due to opioids (a class of drugs which also directly acts on the ENS) [9]. So while the presence or absence of the ENS does not lead to diametrically opposed gut motility states, it is nevertheless important for proper gut functioning. What exactly the ENS does, however, is not completely known.

One goal of this thesis is to provide more information on what role neurons have on proper gut motility. We use ACh, whose effects on guts is well known, to demonstrate that the new analysis method is consistent with previous studies. We also compare fed zebrafish with unfed zebrafish siblings and document the difference in their gut motility states. Finally, we use a genetic mutant with a reduced ENS known as $ret^{hu2846/hu2846}$ (hereafter referred to as $ret^{-/-}$) and compare its motility with wild-type siblings.

Motivation

The construction of the combined microscope was initially performed under the auspices that our future studies, in particular the role of enteric neurons on gut motility, would require both DICM for videos of gut motility and LSFM for 3 dimensional images of the distributions of enteric neurons (which were fluorescently labeled with genetically encoded fluorophores). The combination worked well; we were capable of reconstructing fluorescent neural structures with the LSFM while also obtaining DICM videos of gut motility (see Figure 6). However, as we began our preliminary investigation on gut motility, we found that attempting to contrast zebrafish with varying states of gut innervation was difficult as none had any noticeably different gut motility phenotypes.

To disentangle this problem, we modified our experimental design in a few ways.

The first was to compare only zebrafish with diametrically opposed innervation states: wild-type fish with healthy gut innervation and mutants which completely lacked an ENS (the $ret^{-/-}$ mutant discussed in chapter 1; more below). A consequence of this was that the LSFM component of the combined microscope was no longer particularly relevant (as there would be no enteric neurons to quantify). Conversely, the continual transitioning between 3D fluorescence scans and DICM movies took a great deal of time, so no longer requiring the use of LSFM enabled us to significantly increase our statistics, which we hoped would help distinguish the subtle differences in gut motility.

We also created an entirely new image analysis suite. A technique popular in gastroenterology literature is quantifying motility via spatio-temporal maps (STMaps) [5, 8, 10, 12]. These maps are created in one of several ways. For zebrafish, STMaps had previously been made by taking pixel intensity averages perpendicularly to the gut-axis, then tracing these averages out over time to create a surface [8, 10, 12]. Despite the values of the surface not corresponding to any particular feature of the gut, coordinated events happen to alter the map in visually noticeable ways, so events such as waves traveling from anterior to posterior along the gut appear as diagonal "streaks" in these maps. We decided early on, however, that such maps would be unsuitable for our work, as we were hoping to capture aspects of gut motility that might change in more subtle ways. So while previous studies had found meaningful differences in parameters such as frequency and wave speed, we felt there were aspects of gut motility that were still being neglected. Therefore, we designed a quantitative gut motility analysis suite which would capture nearly all aspects of motility in a far more comprehensive manner and which could render that information

23

down into new quantitative parameters.

We eventually modified our experimental design further to include studies between zebrafish under different chemical, physiological, and temporal conditions. The first was to use acetylcholine (ACh), a neurotransmitter referenced in chapter 1. We hoped that this chemical would provide a baseline for distinguishing different states of gut motility as it has previously been shown to alter the frequency of motility events [9]. The second additional experiment we performed was comparing unfed and fed fish, hypothesizing that food should play a role in modifying gut motility. Finally, in addition to the original experiment comparing wild-type to $ret^{-/-}$ in videos with 5 minute windows, we also wanted to investigate the changing nature of gut motility over a much longer time (over an hour and a half).

The results of all these experiments, obtained from the new software suite, are provided below and repeated in previously published material [50].

Introduction

Proper gut motility is vital for the health of many organisms, yet measurement and characterization of motility patterns remains challenging, a consequence of both the diversity of gut phenotypes and the limitations of existing analysis and imaging methods. A variety of disorders can alter dynamics of the gut. In humans, for example, inflammatory bowel disease, irritable bowel syndrome, chronic intestinal pseudo-obstruction, Hirschsprung disease, and other ailments typically cause gut dysmotility [2, 51, 52]. Even within a healthy individual, the gut exhibits different types of movements depending, for

example, on its digestive state [53, 54]. When fasting, the gut experiences the cyclic sweeping patterns of the migrating motor complex (MMC) [53, 55, 56]. The presence of food triggers changes in gut movements that in turn affect the ingested material. Standing contractions serve to mix and break up food, for example, and propagating contractions transport contents along the gut [53, 56, 57].

Rhythmic smooth muscle contractions are orchestrated by an interplay between the slow waves of pacemaker-like interstitial cells of Cajal and the enteric nervous system (ENS) [53, 56, 58]. Gut movements arise from coordinated activation of sensory neurons, as well as both inhibitory and excitatory motor neurons that can be activated by mechanical or chemical stimuli, guided also by gut-extrinsic innervation [53, 56]. Although the neuronal circuits and neuronal subtypes that locally regulate contractions have been identified in mammalian models [53, 57], little is known about how these different neuronal subtypes work together to coordinate and switch between all of the complex motions of the gut and how gut motility is influenced at the whole organ level by digestive states or other chemical or physiological perturbations [57, 59].

Our ignorance stems in part from a challenge inherent to the study of gut motility: the gut displays a large variety of dynamic behaviors, yet understanding these behaviors calls for simple and comprehensible characterizations of their parameters. A common analysis method involves the generation of spatiotemporal maps (STMaps) from video data [60, 61]. In a STMap, intensity in a 2D video series is averaged over the short dimension of the gut, giving a one-dimensional measure that varies over time. This is convenient to plot, as the one spatial and one temporal dimension are readily assembled into a two-

dimensional graph. Correlated patterns, such as traveling waves along the gut, appear as streaks in the plot. A STMap enables straightforward determination of three important parameters of gut motility: the peristaltic frequency, the propagation velocity for peristaltic waves traveling along the gut, and the wavelength of contractions [11, 60, 61, 62]. A major limitation of STMaps, however, is that they provide at best only qualitative measures of contraction strength, since the image intensity axis is just a measure of brightness, not a quantitative measure of gut shape or motion. In other words, differences in intensity in an STMap can't be mapped onto measures of the actual magnitudes of gut tissue displacement. The magnitude of contractions is likely to be modulated during both normal gut function and various disease states, thus good measures of this characteristic are needed. More generally, expansion of the repertoire of parameters beyond a basic set of three would allow finer characterizations of different physiological states that are beyond the reach of current methodologies.

In this study, we report a new image analysis technique that returns quantitative measures of gut contraction strength, as well as frequency and wave speed. This approach, described in more detail below, involves applying well-established image velocimetry techniques to videos of gut motility, and analyzing the magnitude of dominant periodic modes via Fourier transformation. The code is freely available on github.

We apply and assess this technique using images of larval zebrafish guts obtained from a custom built differential interference contrast microscope (DICM) [18]. Zebrafish are ideally suited for in vivo imaging due to their external development and optical clarity during embryonic and larval stage. In addition, zebrafish is an important animal model for

26

studying gut development and function, including aspects of human gut diseases [63, 64] and gut microbiota function and dynamics [63, 65]. DICM provides high contrast and high resolution optical sectioning, therefore enabling robust image velocimetry calculations. Our method can be more generally used, however, and should, for example, be applicable to dissected preparations commonly used in studies of mammalian guts. Also, as our method is agnostic as to which type of images are analyzed, it can be used for a variety of cellular movements.

To validate our methods, we examine the effects on larval zebrafish gut motility parameters of a chemical stimulus, a physical perturbation, and a biological deficiency, namely acetylcholine, food, and absence of an enteric nervous system, respectively. We find that acetylcholine-treated larvae show a previously reported increase in contraction frequency [9, 11] as well as a newly reported increase in contraction amplitude. Comparing gut motility parameters in fed versus unfed larvae, we find that feeding increases contraction frequency and sustains higher amplitudes over the observed developmental window. Zebrafish larvae lacking ENS innervation show decreased contraction amplitude and also reduced parameter variability compared to wild-type siblings. In addition, imaging over longer intervals reveals highly variable gut motility patterns within individual zebrafish larvae that appear to be ENS-dependent, as the variability of these patterns is lower in mutants lacking ENS innervation. We suggest that our analysis method opens exciting new avenues for studying gut motility in zebrafish and other systems.
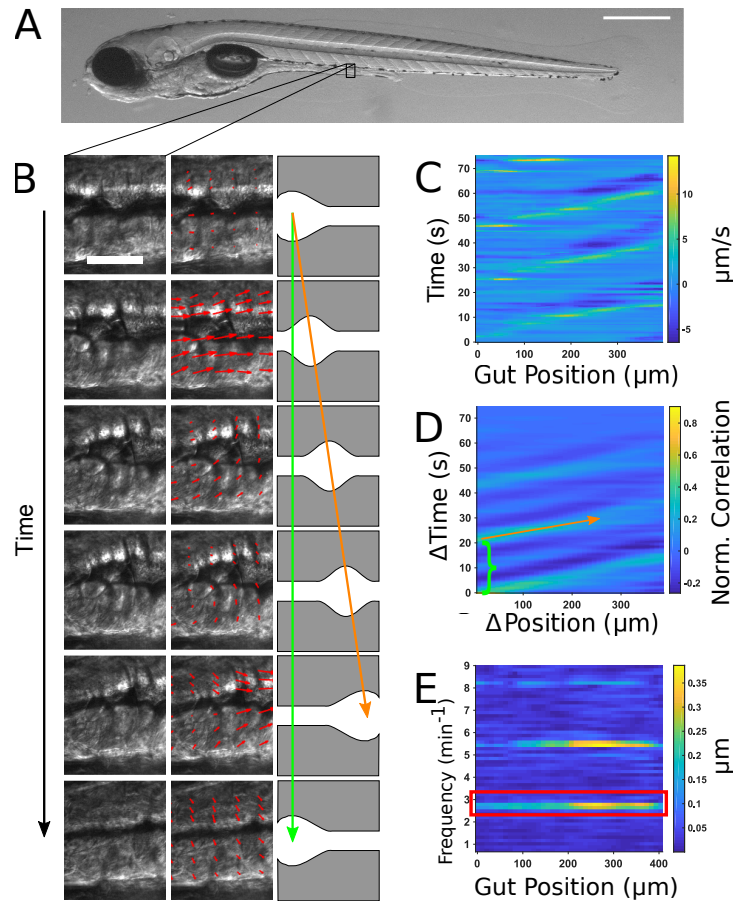
Figure 7. (A) Brightfield image of a 6 dpf zebrafish larva. Scale bar: 500μm. (B)

Left: DIC images of a small region of the midgut. Scale bar 25 μm. Center: the velocity

vector field (red arrows) obtained from running PIV on the image series. Right: schematic

illustration of coordinated movements from left to right (anterior to posterior). Wave speed

is indicated by the slope of the orange arrow and periodicity indicated by the extent of the

green arrow. (C) QSTMap. The color axis represents the velocities, with positive and

negative values denoting posterior and anterior movement, respectively. (D) Cross-

correlation of the QSTMap. The period is given by the green bracket and is analogous to

the length of the green arrow in (B). The wave speed is given by the angle of the orange

arrow and is analogous to the orange arrow in (B). (E) Power spectrum of the QSTMap.

The amplitude is the average of the power spectrum at the motility frequency (red box).

Results

An image analysis technique based on quantitative spatiotemporal maps and
spectral analysis identifies gut motility parameters

To distill complex images of gut motility into concise yet meaningful parameters, we
developed a new image analysis approach using image velocimetry and spectral analysis
(Fig. 7). A typical zebrafish imaged at 6 days post fertilization (dpf) is shown in Fig. 7A. A
full description of the technique can be found in the Materials and Methods section; we
provide a summary here. In our experiments, videos of zebrafish gut motility were obtained
with DICM (Fig. 7B, first column). A velocity map of the material in each image in the
series was determined by digital Particle Image Velocimetry (PIV) [66]. We used well-
established and freely available PIV code [67] that divided each image into a grid of sub-
images; the sub-image pairs in adjacent frames that were maximally correlated with each
other revealed the frame-to-frame displacement of material in that region, or equivalently
its velocity (Fig. 7B, second column). Areas outside the gut were discarded from the
analysis.

Because we were primarily concerned with motion along the anterior-posterior
(AP) axis, and its variation along that axis, we considered only the AP components of the
resulting two-dimensional displacement map, and further condensed these by averaging
along the dorsal-ventral axis (DV). We thereby obtained a one-dimensional curve
representing the instantaneous AP frame-to-frame displacement of gut tissue as a function
of the distance along the gut. Evaluating this over time, we generated a quantitative
spatiotemporal map (QSTMap) of AP displacement as a function of AP position and time

29
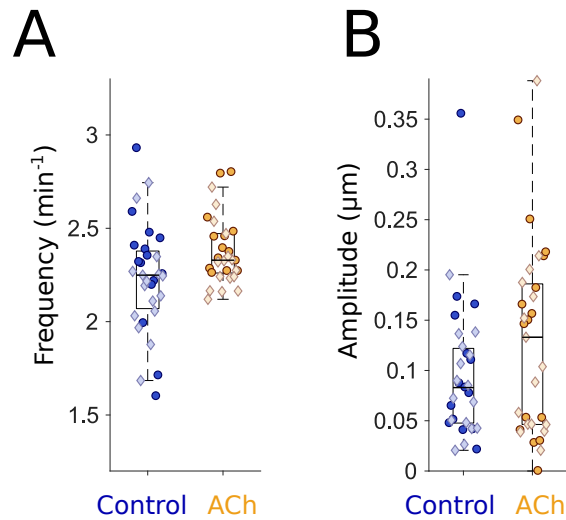
Figure 8. Acetylcholine alters the amplitude and frequency of gut motility. (A) Gut motility frequencies for 6 dpf control larvae (blue, n=31) and larvae immersed in 2.5 mg/ml acetylcholine (ACh; orange, n=30), showing an increased frequency in ACh-treated larvae (mean ± s.e.m. = 2.38 ± 0.0331 min-1) compared to untreated controls (2.23 ± 0.0527 min-1). Each point represents data from a five minute video of a single larva, captured at 5 frames per second. Darker circles and lighter diamonds represent two independent experiments. (B) Gut motility amplitudes corresponding to the same experiments depicted in panel (A). Both the mean and the standard error of the mean of gut motility amplitudes for ACh-treated larvae (0.128 ± 0.0174 μm) are higher than controls (0.0952 ± 0.0121 μm).

(Fig. 7C).

The QSTMap has similarities to STMaps used in previous studies (e.g. [60, 11, 62, 61]). The frequency of gut motility events can be inferred from their temporal spacing (Fig. 7B, green arrow, and 7D, green bracket), and the wave speed is given by the slope of linear features in the map (Fig. 7B, orange arrow, and 7D, orange arrow). Unlike STMaps, the intensity of a QSTMap at any point is not simply a measure of image intensity, but rather
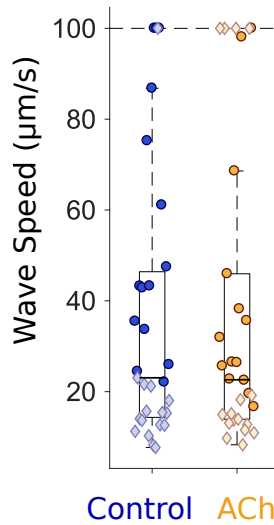
Figure 9. Acetylcholine does not alter the wave speed of zebrafish gut motility. Wave propagation speeds for 6 dpf control larvae (blue, n=31) and larvae immersed in acetylcholine [ACh; 2500mg/l (orange, n=30)]. The dotted line represents a user defined noise ceiling. Each point is derived from a five minute video of a single larva. Darker circles and lighter diamonds represent two independent experiments.

gives the instantaneous velocity, related to the amplitude of motility events, which we make use of below.

To more robustly quantify wave frequency and speed, we calculated the cross-correlation of the QSTMap: at each AP position (x) and time (t), we calculated the product of the QSTMap value and its value at a position and time shifted by (Δx, Δt), and then average over all x and t (Fig. 7D). A wavelike mode of velocity v, for example, will be well-correlated with an image of itself shifted by Δx = v Δt, while random motions will, on average, be uncorrelated. The time shift of the first local maximum at Δx = 0 represents the periodicity of gut motility (green bracket in Fig. 7D). The inverse slope of the peaks in the

cross-correlation map corresponds to the wave speed (orange arrow in Fig. 7D). Parameters such as the wave duration and the variance of wave speed could also be determined.

To characterize the amplitude of gut motility events, not possible with standard methods, we applied spectral analysis to the QSTMap, highlighting periodic signals and quantifying their magnitude. We calculated the one-dimensional Fourier transform of the QSTMap displacement at each AP position (x), decomposing the time-varying function into contributions from each of the range of possible frequencies. The square of the Fourier transform, known as the power spectral density, is composed of strong peaks at the frequencies of gut motility events (Fig. 7E), namely the primary frequency (red box) and its harmonics. We defined the gut motility amplitude as the average of the magnitude of the Fourier transform at the primary event frequency.

Acetylcholine increases the frequency and amplitude of gut motility in zebrafish larvae

The neurotransmitter acetylcholine (ACh) has been shown to increase the frequency of movements in the developing zebrafish gut at several different developmental stages [11, 9]. To test our image analysis method in an experimental setting with an expected outcome, we treated wild-type larvae at 6 days post fertilization (dpf) with 2.5 mg/ml ACh and compared their gut motility with that of untreated siblings. DICM videos were taken at 5 frames per second for 5 minute durations and analyzed as described above. In agreement with Shi and colleagues (2014)[9], frequencies were generally higher for ACh-treated larvae than for controls (Fig. 8A), with mean $\pm$ s.e.m. values 2.38 ± 0.03 min^{-1} and $2.23 \pm$

0.05 min^{-1}, respectively. In particular, only a few ACh- treated larvae showed frequencies that were lower than the median of the frequencies for untreated, control larvae, and the standard deviation of the motility frequencies for ACh-treated larvae was also lower than for the control larvae (Fig. 8A). The ratio of the mean frequencies for treated and untreated larvae in our experiments is 1.07 ± 0.03, clearly greater than 1, as was also the case in Shi et al.'s study in which frequency was assessed from manual counting of occurrences of folds in the gut [9].

To further examine the utility of our program, we extracted information about the wave propagation speed and amplitude of motility events. ACh-treated larvae exhibited no difference in wave speed compared to controls (Fig. 9). However, 2.5 mg/ml ACh increased the median motility amplitude by over 50% (Fig. 8B). The mean ± s.e.m. amplitude values at 0.2 seconds per frame were 0.128 ± 0.0174 μm and 0.0952 ± 0.0121 μm for ACh-treated and control larvae, respectively. Increased larval gut contraction strength has not been reported previously, but is reminiscent of similar ACh-induced effects seen in ex vivo smooth muscle preparations from adult zebrafish [11].

Feeding increases gut motility frequency and sustains amplitude during development

Food is well-known to influence gut motility, in particular by triggering contractile waves often referred to as peristaltic motions [53, 56]. In zebrafish, the influence of food on gut motility patterns has not previously been assessed. We predicted that food-induced contractions would lead to observable and quantifiable increases in motility amplitude. To
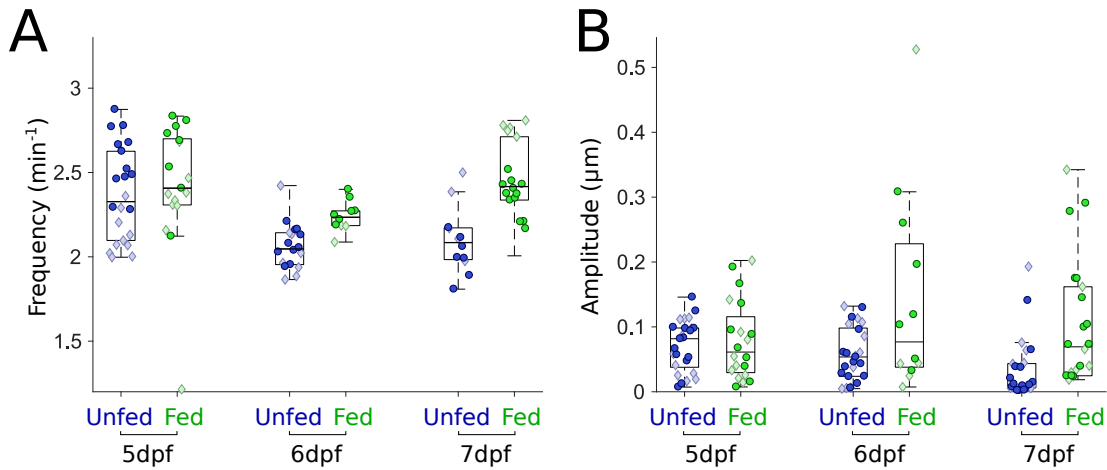
Figure 10. Feeding increases the frequency and amplitude of gut motility. (A) Gut motility frequencies for unfed (blue, n=22,18,12) and fed (green, n=17,10,18) larvae over three days of development. Frequencies of fed and unfed larvae remain similar after one day of feeding. Frequencies become different over the next two days, with fed larvae showing higher frequencies. Darker circles and lighter diamonds represent two independent experiments. (B) Gut motility amplitudes corresponding to the same experiments depicted in panel (A) for unfed (blue, n=25, 25, 25) and fed (green, n=20,12, 22). As in panel (A), amplitudes are similar to one another one day after feeding but the means become significantly different over the next two days.

test this hypothesis, we compared gut motility parameters in both fed and unfed siblings over three days of development from 5-7 dpf. As before, 5 minute DICM videos were taken at 5 fps and analyzed. Videos in which food pieces were evident within the gut were discarded, as velocimetry is unable to distinguish cellular movement from food movement.

We compared gut motility frequency (Fig. 10A) and amplitude (Fig. 10B) in both fed and unfed siblings. Surprisingly, we found that feeding larvae alters the frequency of
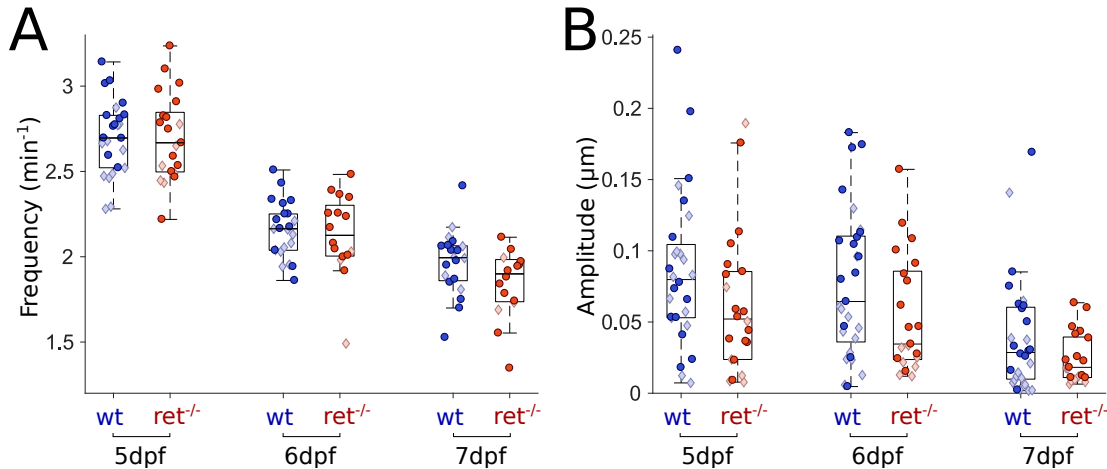
Figure 11. *ret* mutants lacking an ENS display similar frequencies and reduced amplitudes compared to wild-type siblings. (A) Gut motility frequencies for wild-type (wt) (blue, n=25, 23, 20) and *ret⁻ᐟ⁻* (red, n=21,16,16) larvae over three days of development. Frequencies of *ret⁻ᐟ⁻* and wt siblings are the same over three days of development. Darker circles and lighter diamonds represent two independent experiments. (B) Gut motility amplitudes corresponding to the same experiments depicted in panel (A) for wt (blue, n=28, 29, 28) and *ret⁻ᐟ⁻* (red, n=22, 21, 21). Amplitudes and standard deviations of those amplitudes of *ret* mutants are consistently lower over all three days compared to wt.

gut motility. At 5 dpf, there is little difference between fed and unfed larvae (Fig. 10A). However, for the next two days of integrated food consumption, fed gut motility frequency diverges away from that of unfed siblings (2.24 ± 0.03 min⁻¹ and 2.06 ± 0.03 min⁻¹ for 6 dpf fed and unfed, respectively, and 2.45 ± 0.06 min⁻¹ and 2.10 ± 0.06 min⁻¹ for 7 dpf). Strikingly, whereas unfed larvae appear to have monotonically decreasing frequency with age, fed larvae show higher gut motility frequency at 7 dpf than at 6 dpf (Fig. 10A).

As expected, zebrafish gut motility amplitude increased with feeding, though in an
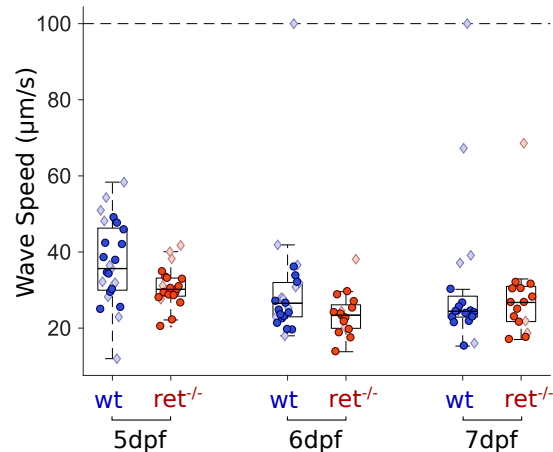
Figure 12. *ret* mutant zebrafish larvae show no noticeable difference in gut motility wave speed compared to wild-type (wt) siblings. Wave propagation speeds for wt (blue, n=25,23,20) and *ret*$^{-/-}$ (red, n=21,16,16) larvae over three days of development. The dotted line represents a user defined noise ceiling. Each point is derived from a five minute video of a single fish. Darker circles and lighter diamonds represent two independent experiments.

age-dependent manner (Fig. 10B). At 5 dpf, after one day of feeding, little change in amplitude is evident (Fig. 10B). However, for the next two days of integrated food consumption, the amplitude difference between fed and unfed larvae increases, with the median value in fed larvae being 1.4 times greater than in unfed larvae at 6 dpf, and 6.5 times greater at 7 dpf. The mean ± s.e.m. values were 0.143 ± 0.045 µm and 0.058 ± 0.008 µm for fed and unfed larvae respectively at 6 dpf, and 0.103 ± 0.021 µm and 0.033 ± 0.009 µm at 7 dpf. At both 6 and 7 dpf, feeding also leads to an increased spread in the amplitude data (Fig. 10B).

Larvae lacking ENS innervation display decreased motility amplitude

Changes in ENS innervation are known to affect gut motility [14, 68, 69]. We analyzed gut motility parameters in 5-7 dpf $ret^{hu2846/hu2846}$ (hereafter referred to as $ret^{-/-}$) mutants. These fish lack ENS innervation and serve as models for Hirschsprung disease, a human congenital disorder. Surprisingly, we found no discernible difference in frequency (Fig. 11A) or wave velocity (Fig. 12), in contrast to a recent study reporting reductions in these parameters in 7 dpf *ret* mutant larvae [14]. However, we found that on average, zebrafish *ret* mutants show reduced gut motility amplitudes compared to wild-type siblings at all days examined (Fig. 11B). We have previously noted the lower motility amplitude of *ret* mutants, using an early version of this analysis approach [65].

Variability in gut motility parameters is dependent on the ENS

The amplitudes of gut motility events show considerable variability between individuals, especially among wild-type larvae (Fig. 11). We hypothesized that this variability would also be manifested within individuals over longer observation times, and that it would be larger in wild-type than in *ret* mutant larvae. To test this hypothesis, we imaged 6 dpf larvae for approximately 90 minutes, and analyzed the resulting gut motility patterns as described above, generating spectral signatures of 4 minute sliding windows spanning the full duration of the movies (Fig. 13A,B). We found that wild-type larvae show a remarkable range of amplitudes over time both within and between individuals (Fig. 13A,C). In comparison, *ret* mutant larvae display much less amplitude variability within individuals (Fig. 13B,D).
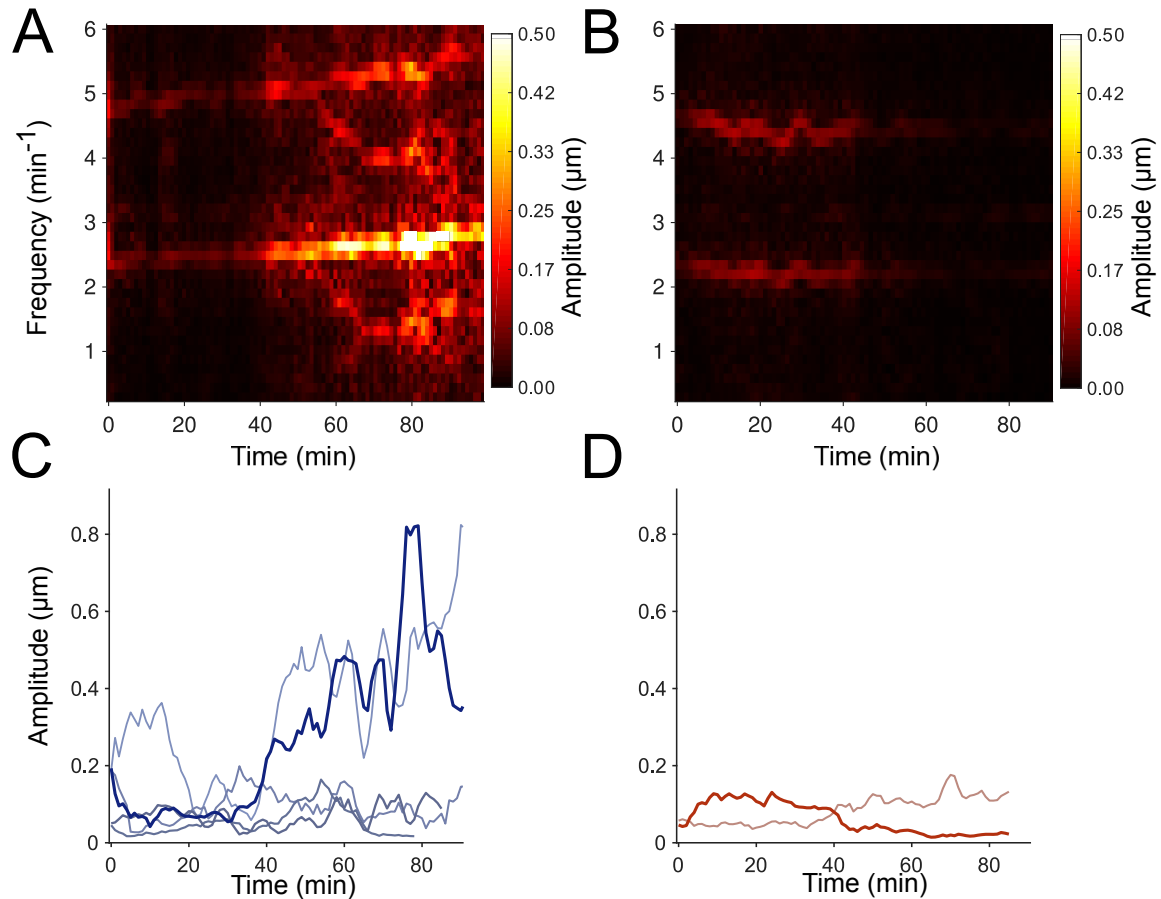
Figure 13. Wild-type larvae have higher amplitude variability than *ret* mutants. (A) Spectrogram illustrating the time-varying gut motility power spectrum of a wild-type (wt) larva over 1.5 hours. Each column depicts the power spectrum calculated over a 4-minute window. (B) A spectrogram of a single *ret* mutant larva. (C) Maximum Intensity Projections (MIP) of spectrograms for wt larvae (n=5); each curve represents a different larva. The bolded blue curve is the MIP of the spectrogram provided in (A). (D) MIP of the spectrograms for *ret* mutant larvae (n=2). The bolded red curve is the MIP of the spectrogram provided in (B). The amplitudes for both *ret* mutant larvae are lower and less variable over time than most wt larvae.

Discussion

The complex motility patterns of the vertebrate gut are crucial to its function, and are modulated by developmental processes, physical and chemical stimuli, and the pathology involved in a variety of disease states. The question of how to measure and characterize gut motility in a way that captures its essential features is therefore both important and timely.

Periodic, propagative contractions are critical for gut activity. For any periodic oscillatory motion, frequency and amplitude are essential and distinct characteristics. It has long been realized that data from imaging studies can readily yield gut motility frequencies and related properties such as wave propagation speeds, for example via image-derived STMaps. Straightforward yet robust amplitude measures have proven more challenging to obtain. We therefore developed and assessed a new image analysis approach that combines image velocimetry, commonplace in studies of fluid dynamics, and spectral analysis, ubiquitous in signal processing applications, to provide quantitative measures of parameters related to both frequency and amplitude.

We apply this approach to data derived from DICM imaging of the larval zebrafish gut. DICM is well-suited to this analysis as it provides high contrast images of sub-cellular features as well as intrinsic optical sectioning. The former facilitates image velocimetry, as there are abundant features to correlate between video frames, while the latter avoids blurring and averaging over the depth of the sample.

We assessed our method in known as well as novel settings including ACh

treatment, comparing fed to unfed zebrafish larvae, and analyzing zebrafish mutants lacking ENS innervation. Previous studies using conventional STMaps have found differences in parameters such as gut peristaltic frequency and the speed at which peristaltic waves travel along the gut for various phenotypes [8, 14, 69] and experimental conditions [10, 11, 70]. We have shown, however, there exist phenotypes that are identical in frequency or wave speed that are nonetheless different in the amplitude of gut motility, highlighting the importance of examining this axis of behavior. In addition, even for known experimental settings like treatment with ACh, we found that in addition to the expected increase in frequency, the amplitude of gut movements is also increased. Our program allows a more comprehensive analysis of gut motility parameters. Furthermore, the framework of cross- correlations, spectral analysis, and open-source software enables additional parameter extractions, if desired. The image analysis method presented here quantifies imaged motions in an automated and reproducible manner. In addition, it is agnostic to the types of images it analyzes, making it versatile for a variety of cellular movements.

Due to the indiscriminate and automated nature of the analysis, a wider range of movements will be recorded when compared with methods that make use of manual feature identification. Consequently, some of the parameters defined in this study may not correspond directly to parameters obtained in previous research. As an example, previous studies have defined the frequency of gut motility only when a sustained wave travels along a large enough distance of the gut. In contrast, our method will identify the frequency of any periodic motion, whether it is a standard motility event or a single muscle cell firing

wild-type sibling	ret⁻/⁻
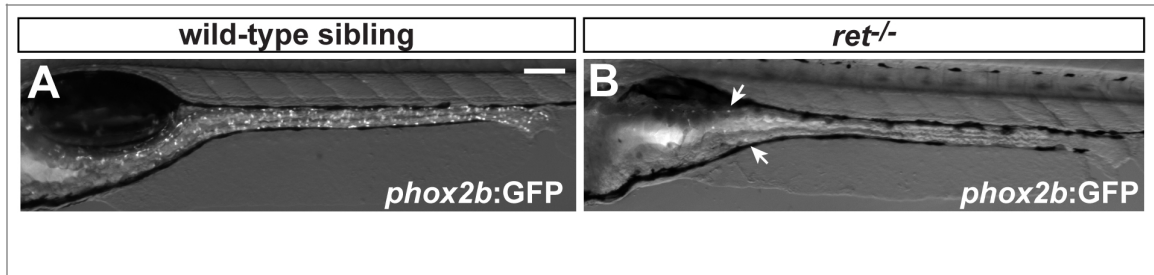
Figure 14. *ret* mutant zebrafish larvae lack ENS innervation. Lateral views of 6 dpf sibling larvae, from combined brightfield and fluorescence images. (A) A wild-type larva with ENS neurons expressing GFP driven by the *phox2b* promoter (*phox2b*:GFP) along the whole gut. (B) A *ret* mutant larva, which lacks ENS innervation except few GFP positive ENS neurons in the anterior-most part of the gut (arrows). Scale bar = 100μm in A, B.

repeatedly. In future applications, the user could define their own parameters from the QSTMap or from even the raw velocity vector field.

Our observation of increased gut motility frequency and amplitude in fed, compared to unfed, larval zebrafish provides the first assessment of how feeding alters motility in these animals. It is well-known in general that specific gut movements are triggered by food [53, 56]. In mammals, the gut either displays stationary contractions that are non-propulsive and are necessary for mixing food or propulsive contractions that transport gut contents [53, 56]. Our findings point to rich dynamics that can be rigorously studied in zebrafish, varying for example the duration and type of feeding. Food may also shape the microbial composition of the gut, as recent work has shown that apparent inter-microbial competition can be governed by gut motility [65] and that mutants with altered motility assemble communities that can be distinguished by abundance of particular members [71].

Our examination of gut motility parameters in *ret* mutant zebrafish larvae lacking ENS innervation highlights both the utility of our analysis and the complexity of mechanisms underlying gut motility. Heanue and colleagues [14] examined gut motility parameters in 7 dpf *ret* mutant larvae and found reduced frequency, contraction distance and contractile velocity compared to wild-type siblings [14]. In contrast, our study found a noticeable difference in amplitude but did not find differences in frequency or speed between 5 dpf and 7 dpf. The mutant allele used in these two studies is the same (*ret^hu2846*) and the mutant larvae show the same phenotype regarding enteric neurons, namely a total lack of neurons except few in the intestinal bulb (Fig. 14) [14]. However, the two mutant lines have been maintained on different wild-type backgrounds [Tubingen Longfin, [14], AB (our study)]. Additionally, in contrast to the study of Heanue and colleagues [14], we do not observe an ENS phenotype with fewer neurons and altered gut motility in heterozygous larvae. One possible explanation for the difference in the gut motility defect is differences in the genetic background due to differences in the wild-type lines, most likely related to the high degree of heterogeneity in the number of SNPs between different genetic backgrounds [72]. Interestingly, this difference is very reminiscent of Hirschsprung disease, a genetically complex disorder that displays significant phenotypic variation, for example differences in the extent of intestinal aganglionosis, even among individuals with the same mutant alleles [2]. These results highlight the importance of detecting complementary and independent gut motility parameters, as in our *ret* mutants on the AB background only amplitude was affected. If we had analyzed our data using established methods, we would have concluded that gut motility parameters did not differ between in

ret mutant larvae and their wild-type siblings. Thus, this newly developed approach provides additional parameters that may be differentially affected in different enteric neuropathies or gut diseases.

Phenotypic variation is a hallmark of ENS diseases such as Hirschsprung disease. We observe in general a striking degree of variability within and among individual zebrafish larvae with regard to gut motility amplitude (Fig. 13). This variability is displayed in all the data measurements, but becomes most apparent during longitudinal imaging. It has been previously reported that the speed of gut transit varies considerably among individuals [13]. We suggest that the variability represents different gut motility modes that reflect different gut states at any given time point, for example the difference between when food is being mixed and when nutrients are being absorbed, which is then reflected in amplitude differences. Whereas two of the larvae shown in Figure 13 show strong, varying increases in amplitude, the three other larvae show moderate changes in amplitude. In contrast, *ret* mutant larvae show very little change in amplitude over time. The ENS provides the intrinsic gut innervation that regulates gut movements [53]. We propose that these amplitude changes are regulated by the ENS and may thus be absent from *ret* mutant larvae, motivating future work to establish connections between gut motility modes and specific ENS neuronal activity, and their alteration in the course of gut diseases.

Materials and Methods

Zebrafish Husbandry

All experiments were carried out in accordance with animal welfare laws,

guidelines and policies and were approved by the University of Oregon Institutional

Animal Care and Use Committee. Wildtype and ret^{hu2846} embryos were allowed to develop

at 28.5°C and staged by hours post fertilization according to morphological criteria [73].

Wild-types and ret^{hu2846} were of AB background.

Imaging Experiments

Specimen mounting was performed as described previously (Jemielita et al., 2014).

Briefly, larvae were anesthetized in 80 μg/ml tricaine methanesulfonate (Western Chemical,

Ferndale, WA) for several minutes at 28°C. Larvae were then immersed in a liquified 0.5%

agar gel (maximum temperature 42°C) and drawn into a glass capillary. The gel, once

solidified, was mounted onto a microscope imaging chamber containing embryo medium

(EM) with 80 μg/ml tricaine methanesulfonate maintained at 28°C. The solidified gel and

the larva were extruded into the imaging path to prevent the capillary glass from interfering

with imaging. The mid-region of the gut was imaged, approximately 200 μm anterior of the

anus (vent).

Imaging was performed using a custom-designed and custom-built microscope

capable of differential interference contrast microscopy as well as light sheet fluorescence

microscopy [18]. The specimen was illuminated by a polarized 447nm LED (Quadica

Developments Luxeon Star Brantford, Ontario, Canada) and imaged using a standard

microscope objective (Zeiss Oberkochen, Germany DICMMPlan Apochromat, 40x/1.0). A

Nomarski prism and polarizer were oriented in such a way as to provide Differential

Interference Contrast (DIC) [18]. The resulting image was then focused onto a sCMOS

Camera (Cooke, Kelheim, Germany, pco.edge). Movies were taken with 1 ms exposure times at 5 frames per second.

Acetylcholine treatment

Wild-type larvae were raised in EM until 6 dpf. Acetylcholine treatments were essentially performed as previously described [9]. Briefly, larvae were individually transferred to EM containing either 0.5% DMSO or 0.5% DMSO with Acetylcholine Chloride (Sigma-Aldrich, A6625; 2.5 mg/mL). Larvae were exposed to these conditions for a total of 20-30 minutes, anesthetized with tricaine for several minutes at 28°C, and mounted for imaging as described above.

Feeding of zebrafish larvae

Wild-type larvae were raised in EM until 4 dpf and transferred to embryo medium at 5 ppt salinity (E5) in a new dish and rotifers added to the dish. Fresh rotifers were added at 5 dpf and 6 dpf, so the fed zebrafish larvae had food *ad libidum*; 7 dpf fish were provided food for three days. Larvae were examined to ensure they had no food in their gut immediately prior to imaging, as PIV may track gut contents, such as food, instead of the gut wall.

Particle Image Velocimetry (PIV) and Quantitative Spatiotemporal Maps (QSTMaps)

PIV is a well-established image analysis technique that takes as its input a set of

images and outputs a corresponding set of velocity vector fields representative of the motion contained within those images. To perform PIV, we used publicly available software called "PIVLab [http://pivlab.blogspot.com] in addition to several home-built Matlab programs. A comprehensive description of how PIV works, its many different implementations, and how it is optimized can be found elsewhere [66]. However, a simple example, representative of the key features of the technique, is as follows: A two-dimensional image $I_p(x,y)$ (known as an interrogation area, possibly the subset of an even larger image) at frame p of an image series is subdivided into a grid. We denote the subset of $Ip(x,y)$ centered at grid element (i,j) as the template $t_{pij}(x,y)$. For each template in frame p, the cross correlation in the frame (p+1) is calculated:

$$C(x',y') = \sum_x \sum_y t_p(x,y) I_{p+1}(x-x',y-y')$$

The location of the maximum of C(x',y') gives the most likely displacement of that template neighborhood from one frame to the next. This is repeated over all grid elements to generate a displacement or velocity vector field, and then is repeated over all pairs of frames.

For this study, we used a first pass template size of 32 pixels corresponding to 20.8 microns in the image plane. Preliminary preprocessing consists of using PIVLab's built in PIVlab_preproc function, using contrast enhancement (CLAHE, size 50) and a high pass filter (size of 15 pixels). PIVLab then performs PIV over the entire image, segregating the resultant velocity vector field into a grid whose vertices are separated by 32 pixels. After

46

this processing, a user defined mask is applied to the region of interest (in our case, an area containing the gut) and vertices outside of the mask are discarded.

As the geometry of the gut is not conserved in space or between individual larvae, masking results in the remaining vertex positions and numbers being spatially inconsistent from one data set to another and difficult to deal with numerically. To manage this, a new grid is generated to better accommodate the unique geometry. This new grid has a constant number of rows and columns and is distributed inside the mask in such a way as to fill most of the area. To do this, a curve is drawn by the user which represents the centerline of the mask (not necessarily the geometric center; in our case, the gut lumen). At each discrete position along the curve (equal in distance to the original PIV spacing), a constant number of vertices is distributed orthogonal to the curve at that position. This results in axes which, while spatially varying, are a better representation of the DV and AP axes of the gut. The original velocity field is transformed to the new grid by bilinear interpolation and is its components are projected into the local DV and AP components.

We generate a QSTMap from the resulting velocity field. We are primarily concerned with the AP component of motion, and its variation along the AP axis. We therefore average the AP component of the frame-to-frame displacements along the DV direction, resulting in a one-dimensional map of displacement as a function of AP position, for each point in time. Plotting these functions over time gives the QSTMap. A representative data set is shown in Figure 7C. We note that other analyses are possible, for example considering DV displacements, which can be implemented by modifying our code.

Cross-Correlation Plots Define Frequency and Wave Speed

Larval gut motility waveforms can be individualized and complex. For most cases, the velocity waveform does not have a well-defined set of maxima that can clearly be followed across position and time. These waves, however, often have similar structures that repeat over time. Because of this, we take the QSTMap, Q(x,t), and apply the cross correlation:

$$C(dx, dt) = \sum_{x=0}^{L(dx)} \sum_{t=0}^{T(dt)} \left(\frac{1}{L(dx)T(dt)} \right) Q(x,t)Q(x - dx, t - dt)$$

where t_{max} is the maximum time examined, and $L(dx) = L_0 - dx$ is the length of the gut that can be examined for a given offset dx, and L_0 is the total AP length of the analyzed gut segment, typically around 400 μm.

An example of the resulting cross correlation is shown in Figure 7D. Even for multi-modal waveforms, the cross correlation results in a well-defined set of maxima that linearly increase over changes in distance. Therefore, we find the locations of the maximum of C and fit it to a line. The inverse slope of this line (Figure 7D, orange arrow) is defined as the wave speed.

The first non-zero peak in the autocorrelation of a signal is the time at which velocities at any position in the gut are most similar with themselves. The location of this peak therefore provides a robust measure of the frequency (Figure 7D, green bracket).

<u>Spectral Analysis Defines Amplitude</u>

To define amplitude, we needed a measure that is robust against noise and that focuses on the periodic peristaltic events and ignores occasional large vectors that result from motions such as larvae moving. We therefore perform a Fourier Transform of our QSTMap at each AP position, transforming each $Q_x(t)$ into a function of frequency, f, rather than time:

$$Q(f) = \sum_{t=1}^{N} Q_x(t)e^{-2\pi i \cdot (t-1)(f-1)/N}$$

To obtain the signal strength ("power") at any frequency, we take the modulus (the signal multiplied by its complex conjugate) of $Q_x(f)$. Having previously found the frequency of gut motility from the cross correlation, we define the amplitude as the square root of the power at the frequency of gut motility. For simplicity, our analysis considers only the average of these values over the entire gut in the field of view. Figure 7E shows the resultant power spectrum of the QSTMap from Figure 7C with the red box outlining the peak power at the frequency of gut motility.

The next chapter discusses preliminary engineering efforts undertaken to obtain better statistics for our research. The number of data points for nearly all figures shown so far (e.g. Fig. 10) would likely be able to be increased were we able to increase the throughput speed of the imaging process. Other data which is more rate-limited by the imaging (e.g. Fig. 13) could nonetheless also benefit from this system if it included automation. For these reasons, the next chapter discusses a system we created for the automated, high-throughput imaging of zebrafish.

CHAPTER IV

HIGH THROUGHPUT AUTOMATED MICROSCOPY

This chapter contains unpublished material which will be coauthored with Savannah Logan, Christopher Dudley, Michael Taormina, Teddy Hay, and Raghuveer Parthasarathy. Savannah Logan prepared and maintained biological samples, performed experiments, and designed the preliminary optical setup. Christopher Dudley designed the fluidic system, designed the imaging chamber, modified some optical arrangements, and performed experiments. Michael Taormina built the original fluorescence microscope. Teddy Hay designed imaging analysis software and performed analysis. I built a brightfield microscope, designed electronics for instrument control and data acquisition, designed and wrote software for running experiments and for communicating with and controlling all instrumentation, and performed experiments. Raghuveer Parthasarathy was the principle investigator for this work.

Introduction

For the data presented in this thesis, indeed as well as many other biological and biophysical studies, there is often a large amount of variance that makes distinguishing signals difficult. This variance is often not the result of measurement noise, however, and is instead often actual variation within zebrafish populations. This point underscores the importance of rationalizing what can be considered "significant." For instance, if the distribution of some quantity representing health is slightly offset in mean between two

populations, the real-life consequence of this difference is a higher frequency of health problems in one of the populations, even if the signal is highly variable, i.e. "noisy." In practice, however, we do not know *a priori* that the mean values actually differ between the populations, but rather we work backwards from discrete sets of measurements taken with finite resolution. The question, then, becomes whether one can distinguish false mean differences, which are only present because of finite sampling, from differences that truly result from distinct population characteristics.

This is a difficult question to answer, in general, and a lot has been written about statistical approaches to tackling it. An extremely good answer, however, is to take more data so that our understanding of the underlying distribution becomes more defined. This has the added benefit of potentially revealing distinct sub-populations, unusual distributions, etc.

Of course, acquiring more data isn't trivial. Naively, one might look at the figures presented in this thesis and ask, "Why didn't you just stay longer and collect more data?" Despite the obvious ethical depravity of such a heinous request, this simply does not work with the types of experiments we perform: zebrafish are rapidly developing during this time frame (so 5 dpf is different from 6 dpf), they have physiological cycles (such as sleeping), and they have limitations as to how often they can be mated. Thus, even if experiments were extended later into in the night/morning, the integrity of the data would possibly be compromised.

The solution, of course, is to image faster, either by being more efficient (impossible) or by building a robot whose labor and emotional sensitivities we *can* exploit.

Our current method of manually mounting and finding samples allows us to image (with LSFM) either 6 fish continuously over 18 hours, or, if screening (imaging one fish after another), a maximum of around 10 fish per hour. If the specimen handling was automated and/or it was faster, we could imagine imaging at several times that rate, say 30 fish an hour.

Various automated live-specimen microscopy systems have already been developed, from an automated confocal and brightfield microscope system [74] to an automated LSFM [75]. Neither of these solutions provide an increase in speed. Confocal is, by its very nature, slow, and imaging the volumes we usually image would require a significantly larger amount of time than simply manually mounting the specimens with our setup. And the automated LSFM system images no faster than our own manual mounting. For these reasons we are interested in creating an automated, high-throughput combined LSFM and DICM. To do this, we need to create and combine an automated fluidics system with imaging optics.

There are several design constraints we need to consider. First, we need to load larval zebrafish from flasks without manual intervention and without damage, a task surprisingly non-trivial. We then need to detect when fish are close to the imaging region and, once they are within the field of view, discriminate fish from debris such as bubbles. We need to be able to move a zebrafish, whose cross sectional diameter is a few hundred microns, along several meters of tubing. This distance is necessary to provide optimal spacing between fish. We need to position them to within ~10μm precision (sufficient for robust observation of particular anatomical features, such as the gut or enteric neurons). All
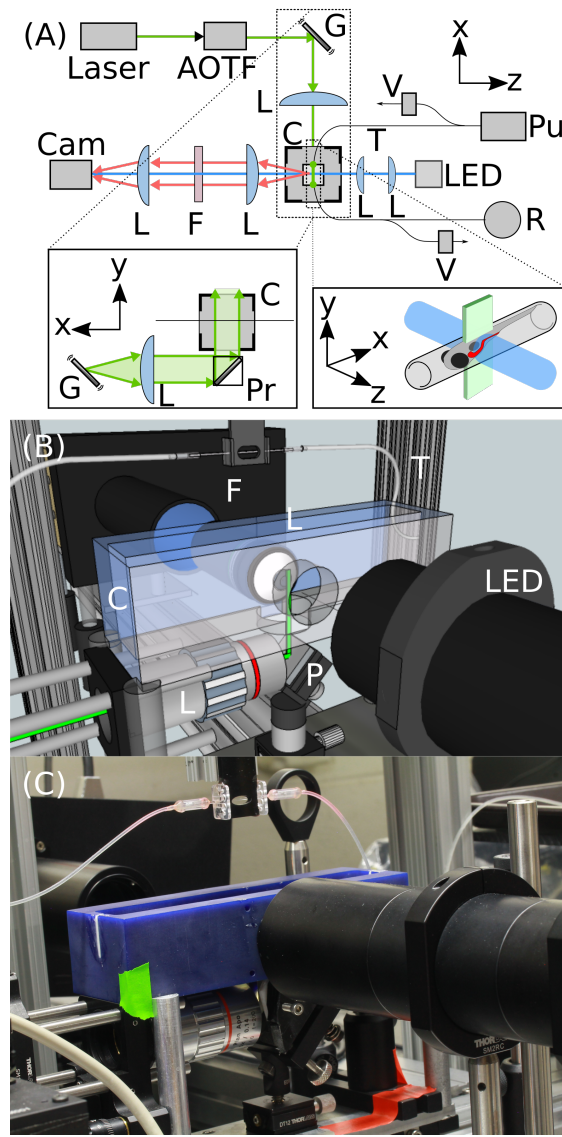
Figure 15. A combined light sheet fluorescence and brightfield microscope capable of automated rapid zebrafish imaging through the use of a fluidic circuit. (A) Block Schematic, Pu=Syringe Pump, V=Valves, R=Reservoir, G=Galvometer, L=Lens, Pr=Prism, C=Chamber, F=Filter Wheel, T=Tubing, Cam=Camera, LED=Light Emitting Diode, AOTF=Acousto-Optical Tunable Filter. (B) 3D Model of the physical setup with components labelled. Note that the orientation for the imaging axis is reversed and that some components are absent from this representation. (C) Physical Setup.

these things need to work while making the system resilient to natural variation and differences in experimental designs (e.g. feeding fish will alter their anatomy compared to unfed, resulting in different fluid mechanics).

For the optics, we need to be able to do LSFM, a technique that uses a unique imaging geometry and which requires ~1μm alignment precision of the sample, the laser sheet, and the working distance of the objective, in a way that is tolerant of the large variability mentioned above. And to top it off, we need to manage the coordination and timing of a large number of instruments in a way that is predictive and tolerant to a variety of different experiments in the future. Below I'll present the preliminary work we've done to achieve this goal. It should be noted that this work is not finished and will continue to be improved even after this dissertation.

Experimental Design

Our instrument integrates computer-controlled fluidics, consisting mainly of pumps, valves, tubing, with light sheet excitation and detection optics. Automating the specimen handling requires abandoning the previous chapter's practice of mounting larval zebrafish in gel. Instead, zebrafish are serially drawn into a line of tubing, often several meters long, to later be pushed directly into a glass capillary directly in the field of view of the camera. After the imaging is performed, zebrafish are pushed out of the line and back into a dish or flask, similar to previous experiments.

Our setup is shown in Figure 15. The fluidics [Fig. 15(A)] consist of a computer

controlled syringe pump (Pu) (KDScientific, Holliston, MA, Legato 111) which infuses a

tubing line (T) with embryo media containing 80 μg/ml tricaine methanesulfonate (Western

Chemical, Ferndale, WA) to inhibit muscle twitching. Two computer controlled pinch

valves (V) (Cole-Parmer, Vernon Hills, IL, 5PSI 12VDC) open and close to control into

which path the fluid flows. The two main modes of operation are for stopping a fish to

image and for pushing the fish further downstream. A glass capillary is used for imaging

and is UV-glued on both ends to the flexible tubing via custom plastic fittings. It is placed

into the chamber (C) and controlled by a computer controlled three-axis positioning stage

(Applied Scientific Instrumentation, Eugene, OR). Once imaging the fish has been

completed, the fish is flowed further downstream and back into a flask or reservoir (R).

The configuration for the optics, also shown in Fig. 15(A), is similar to the

configuration described in Chapter II with one exception. The capillary holding the fish is

oriented horizontally rather than vertically, as fish in free flowing fluids will often sink or

float if placed in a water column. Because of this, the laser does not go into the side of the

chamber, as is necessary for vertically aligned samples [Fig. 1(B), inset]. It is instead

directed upwards from below the chamber via a prism (PR), as is necessary for horizontally

aligned samples [Fig. 15(A), inset].

The software used to control all of these optics and fluidics was written in Matlab.

We chose Matlab because we needed a language that was capable of being scripted, was

familiar to the rest of the members in lab, was able to have a Graphical User Interface

(GUI), and which interfaced with all of our hardware. And in addition to providing an

immense versatility in function, such as data analysis, hardware communications,

simulations, and more, Matlab also has an immense user base, amazing documentation, and is particularly easy to learn compared to nearly all other programming languages. This allowed us to first write a significant amount of lower level hardware and flow control code, followed by a GUI which end users, such as members of other biological labs, could use without having to learn the scripting language of Matlab. Users simply start the program, manually position the capillary, and set the scan parameters (such as which colors are used, how many fish they want, how many regions they want to scan, and more). The program handles everything else, from all of the hardware communications and state changes to the image acquisition and data management.

The program is designed to repeat a cycle of instructions an indefinite number of times or up until a number of times specified by the user. To start, the user sets the parameters and then starts the scans. The cycle begins as the pump begins infusing, pushing zebrafish through the tubing. The camera is turned on and when a fish passes the field of view, it blocks light. An average of all pixel values for each frame is stored in an array. If the intensity drop between frames is greater than some empirically determined value, this reverses the state of the valves, immediately stopping the fish and diverting the remaining pump head-pressure elsewhere. One could imagine more sophisticated metrics for determining when to stop the fluid, such as qualifying the shape of the intensity array, or using image correlation with a pre-made library of zebrafish images against the current frame acquired, but these methods tend to take significant processing time and our method is fast enough to do live processing.

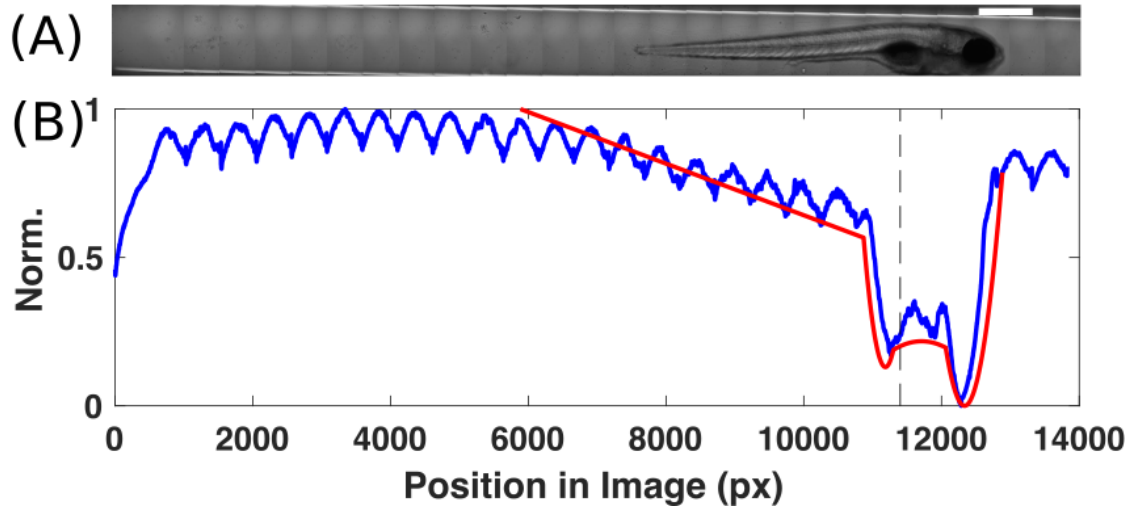Once a fish is detected, a computer-controlled stage moves the capillary

Figure 16. A visual representation of the algorithm used to identify fish and position the stage correctly for imaging. Scale bar = 500 μm. (A) An ensemble of images stitched together, taken by capturing images while moving the stage. (B) The blue curve is obtained by averaging the intensity values in (A) along the vertical direction. Differences between the blue curve and various generated 1D zebrafish profiles (a representative profile is shown in red) are taken at every position and the absolute values of those differences are summed. The curve and position with the smallest difference is used to locate the position and orientation of the fish.

horizontally while the camera collects a series of images along the entire length of the capillary. The software stitches these images together to make a composite image of the entire body [Fig 16(A)]. To determine the position of the fish in this image, and thus real-space, we compare it with a previously made library of representative zebrafish curves (described below). However, we do not do full 2D image correlation, as it is slow and unnecessary, and instead take an average intensity projection along the vertical direction, reducing the stitched image to a 1D mean intensity plot as a function of x [Fig 16(B), blue

curve]. The library of representative zebrafish consists of synthesized 1D zebrafish mean intensities similar to the curve just generated [one representative curve is shown in red in Fig 16(B)]. We score the similarity between these curves by summing the absolute value of the differenced values with the blue curve for all positions and orientations of the red curve. Eventually, the position and orientation with the lowest difference score is taken to be the position and orientation of the zebrafish. We tell the program (in the initialization step) where we want to center the first image [black dotted line, Fig 16(B)] relative to the head of the fish and then move the motorized stage in real space by this amount.

The stage then moves to the initial position and the light sheet begins its scans in whichever colors the user specified. The high throughput software currently has two fluorescence colors available, with laser and filter combinations for excitation wavelengths 488 nm (GFP) and 561 nm (RFP), and these can be used together or separately. Each color scan finishes before the next begins. After the color scans are completed, if the user specified multiple regions, the stage moves to those regions, completing more sets of color scans.

Once all of these steps are finished, the valves open up and the cycle starts anew, pumping fluid and looking for more zebrafish.

Results

We characterized the optical quality of the setup by measuring the instrument's point spread function (PSF). To do so, 20nm GFP fluorescent polystyrene beads were
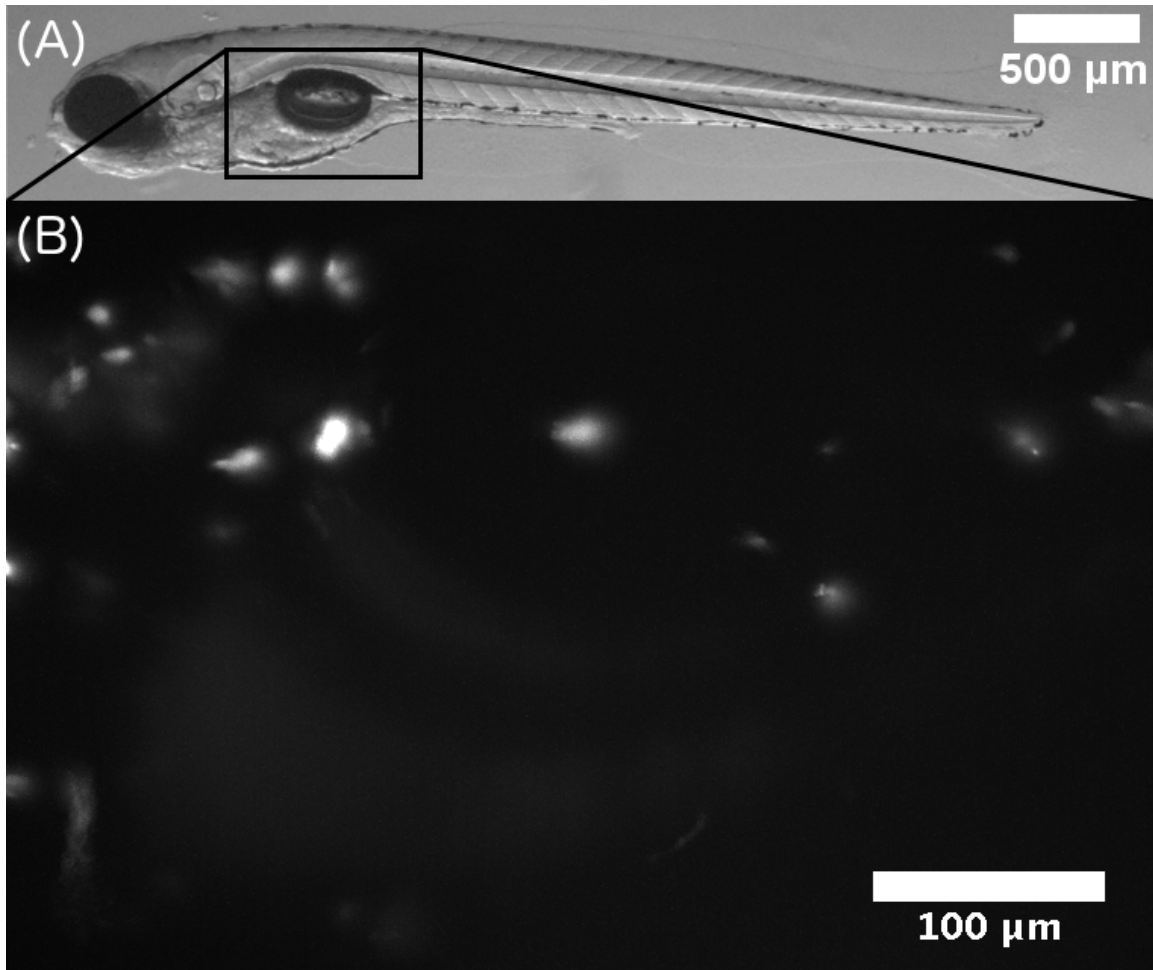
Figure 17. (A) A zebrafish, with panel (B) outlined. (B) a maximum intensity projection of a LSFM scan of a zebrafish with fluorescent neutrophils, obtained with the high-throughput system. The neutrophils are the bright spots and regions in the image.

pipetted into a water index-matched immersion oil at 1:1000 dilution. The mixture was then directly pipetted into the imaging glass capillary and placed into the chamber as usual. Central intensity values for fluorescing beads were taken as we scanned the beads in z. Despite our laser line having a full width at half maximum (FWHM) of only a couple microns, we found that the FWHM of the beads in z was several times larger. This implies that the our system currently has optical aberrations due to the cylindrical glass capillary

and that our PSF is not optimal. We are currently exploring options for fixing this, such as optical corrections upstream to counteract the aberrations or by using thinner tubing.

To assess the instrument's throughput capabilities with respect to live specimens, we assayed the immune response of initially germ-free zebrafish to a population of known gut-microbes. Prior work has shown that the presence of some bacteria species can lead to an increased number of neutrophils (a type of immune cell) surrounding the gut [76]. To determine this, after a period of inoculation with the bacteria, zebrafish guts (length ~1mm) for both germ-free and bacteria associated fish were dissected and the neutrophil cells counted by visual inspection using a stereomicroscope. The study showed that several bacterial species lead to an increased presence of neutrophils surrounding the gut.

These experiments were difficult and time-consuming to perform. With the high throughput system, not only could we possibly automate this counting, but we could do it in a living animal with greater statistics, with greater ease, and over several developmental times. Therefore, we repeated these experiments, using zebrafish with GFP positive neutrophils *Tg(BACmpx:GFP)i114* [76] (referred to as MPO). We derived them germ-free and subsequently inoculated half of them with a population of zebrafish-commensal bacteria (Vibrio, ZWU0020). However, instead of dissecting the guts, we used the light-sheet to obtain the number of neutrophils present within the fish. Figure 17 shows the maximum intensity projection of the neutrophils within a region of the zebrafish gut. The analysis of neutrophil numbers from the images is still in progress.

We were able to get performance benchmarks for our system with this experiment. Note that these numbers are preliminary, from the first run of the complete system, and are

likely to get better: Over three days of imaging, scanning two regions and in two colors each, we triggered 153 events (amounting to 612 full 3D scans, 315GB of data). Eleven triggers were false positives (7%), caused by debris, bubbles, and/or zebrafish that were not fully anesthetized. For correctly triggered fish, there were 27 positioning errors (19%), in which the program didn't correctly identify the orientation of the fish, or there were multiple fish in the field of view. We scanned at a rate of ~60 3D scans/hr at a spacing of 5μm between slices corresponding to 15 fish/hour. The total time per fish was 04:01±00:18 min (N=40). Most of the time was spent imaging: the imaging time was 2:34±00:02 min (64% of the time). The time spent doing positioning calculations was 00:23±00:03 min (9% of time). All other steps (pumping, stage movement, valves tripping, fish finding) took 01:04±00:18 min (27% of time).

The next chapter concludes this thesis and discusses the context of the work presented as it relates to the scientific community as a whole. It also provides some thoughts for extending microscope designs and for continuing and advancing the research we've preformed.

CHAPTER V

CONCLUSIONS AND FUTURE DIRECTIONS

Summary

The material in this dissertation consists of the design and construction of two different microscopes, the creation of a new image analysis software, and the scientific analysis of zebrafish gut motility using those systems. In general, uncovering new knowledge about the universe requires more than just having a curious mind; it also requires having the right instrumentation. The common goal amongst all of the material in this dissertation was to open up entirely new spaces for scientific discoveries through the innovation of new tools.

Chapter II concerned the design and construction of a microscope capable of combining, for the first time, LSFM and DICM. The new microscope provided a new geometry more suitable to imaging zebrafish gut motility. Its combination with LSFM meant that the two imaging modes could be performed in the exact same field of view at the same time and without needing to unmount and re-mount the specimen in exactly the same configuration as it had been previously.

Chapter III described of the creation of a new image analysis software suite and the findings of a study on the gut motility of zebrafish prepared in various states. We originally hypothesized that the gut motility of zebrafish might be altered in subtle yet consistent ways under a variety of different genetic, chemical, and physiological states. In order to extract these subtleties, we designed software which could track nearly every aspect of the

motion, utilizing a standard approach known as particle image velocimetry. The software then focused on only aspects of the gut motion we cared about, such as anterior-posterior traveling waves. Finally, it was able to then project the complex mathematical space onto a few meaningful parameters via mathematical techniques such as cross correlations and spectral analysis.

Parameters obtained from this analysis were shown to have meaningful differences between zebrafish in various states. First, we reproduced data concerning the frequency altering properties of acetylcholine in zebrafish gut motility patterns. However, this analysis also revealed that acetylcholine alters the amplitude of gut motility, which had not previously been shown. We then uncovered the role feeding had in both the frequency and amplitude of gut motility, showing that food caused sustained increases in both parameters when compared to the monotonically decreasing values found in unfed fish. We then found that, in contrast to literature showing otherwise, zebrafish lacking enteric neurons maintained identical gut motility frequencies and only had a mild reduction in gut amplitudes. We were able to show, however, that gut motility amplitudes in wild-type fish were drastically different over longer periods of time when compared to mutants lacking an ENS.

Chapter IV discussed the invention of a new LSFM which automated the rapid imaging of zebrafish. We described the geometry of the system, which differs from that of conventional LSFM setups. We also showed that the effective volume of useful data collected was higher than manual imaging and considerably easier to set-up.

Future Directions

Each chapter of this thesis consisted of the creation of tools which have already begun producing scientific results. It is my hope that these tools continue to be of use and that others utilize and expand their designs. There are several areas for improvement and there are many experiments that were unable to be realized during my time here.

One potentially fruitful avenue of research is in the direct imaging of neural processes. A specific genetically encoded calcium indicator known as GCaMP has previously been used to directly watch neurons fire in the brain of live zebrafish [26, 77]. By modifying the genetics to get GCaMP to work in the ENS, one might be able to use the combined DICM and LSFM to correlate the gut motility vectors obtained from the analysis program directly with the firing of gut neurons (obtained with LSFM). It's possible that gut neurons act directly on cell tissue, in which case a firing neuron would directly correlate with a movement somewhere, or that there is a more abstracted control, in which case activity may still be correlative.

In general, I believe the program I have written for analyzing gut motility will continue to be used. For instance, Savannah Logan, a graduate student who helped with some of the experiments in this thesis, has used the program to analyze the gut motility in zebrafish inoculated with antagonistic bacteria and has found strong strain-dependent motility amplitudes. Kristi Hamilton, a postdoctoral fellow in Judith's lab, has used the program to analyze differences in fish under even more chemical, physiological, and genetic conditions. Our motility software suite is publicly available on a Github repository (https://github.com/rplab/Ganz-Baker-Image-Velocimetry-Analysis)[50]. This opens the

door for a variety of future modifications, including modification by future users outside our lab.

There are a virtually endless number of modifications and improvements which can be made to the software. One major area for improvement is what data gets used. For all analysis done so far, a significant volume of data has been thrown out. Dorsal-ventral components of the PIV vectors are not considered during the analysis, nor is the transversely varying nature of the PIV vectors. One could imagine doing the same analysis on them as was done on the AP components, and entirely new analyses could be performed on the combination, such as quantifying the vorticity of gut motility. In addition, the program is currently specific to zebrafish gut analysis. For instance, user-made PIV masks assume that the system has a symmetry above and below a luminal centerline, something which might not be present in other studies. One can imagine doing studies in completely different systems (e.g. blood flow, different animals) and the program could be minimally modified to incorporate them.

The combined microscope has been and will likely continue to be used for a large volume of other research. It will likely continue to be used for looking at bacterial populations in zebrafish, and gut-microbiome research in general, as well as a variety of other projects, from index-matched sphere packing in fluid, to work with *Drosophila* and other non-zebrafish animals.

The high-throughput LSFM and DICM will continue to be improved in the future. Current projects are limited to imaging zebrafish at randomly determined orientations, which limits some research. This will be fixed in the future by incorporating a rotation

mount which will, in combination with software, be able to orient the fish consistently. The software can also be modified to be more modular, providing further features, from dynamic repositioning in the event the fish moves, to providing options and presets for a variety of different types of experiments. In addition, the system will hopefully include an imaging circuit, a system in which previously imaged fish can be stored for some time and then sent back to the imaging apparatus repeatedly, allowing for longitudinal studies. These are just a few examples of the virtually endless number of changes that can be made to the system.

REFERENCES CITED

[1] B. Mazet, "Gastrointestinal motility and its enteric actors in mechanosensitivity: past and present," Pflugers Archiv European Journal of Physiology, vol. 467, no. 1, pp. 191–200, 2014.

[2] T. a. Heanue and V. Pachnis, "Enteric nervous system development and Hirschsprung's disease: advances in genetic and stem cell studies.," Nature reviews. Neuroscience, vol. 8, no. 6, pp. 466–479, 2007.

[3] J. I. Lake and R. O. Heuckeroth, "Enteric nervous system development: migration, differentiation, and disease.," American journal of physiology. Gastrointestinal and liver physiology, vol. 305, no. 1, pp. G1–24, 2013.

[4] P. G. Dinning, L. Wiklendt, L. Maslen, I. Gibbins, V. Patton, J. W. Arkwright, D. Z. Lubowski, G. O'Grady, P. a. Bampton, S. J. Brookes, and M. Costa, "Quantification of in vivo colonic motor patterns in healthy humans before and after a meal revealed by high-resolution fiber-optic manometry," Neurogastroenterology and Motility, vol. 26, no. 10, pp. 1443–1457, 2014.

[5] G. D'Antona, G. W. Hennig, M. Costa, C. M. Humphreys, and S. J. H. Brookes, "Analysis of motor patterns in the isolated guinea-pig large intestine by spatio-temporal maps," Neurogastroenterology and Motility, vol. 13, no. 5, pp. 483–492, 2001.

[6] W. Sweeney, B. Krafte-Jacobs, J. Britton, and W. Hansen, "The constipated serviceman: prevalence among deployed us troops.," Military medicine, vol. 158, no. 8, pp. 546–548, 1993.

[7] R. R. Simpson, M. L. Kennedy, M. H. Nguyen, P. G. Dinning, and D. Z. Lubowski, "Anal manometry: A comparison of techniques," Diseases of the Colon and Rectum, vol. 49, no. 7, pp. 1033–1038, 2006.

[8] A. Rich, S. Gordon, C. Brown, S. J. Gibbons, K. Schaefer, G. Hennig, and G. Farrugia, "Kit signaling is required for development of coordinated motility patterns in zebrafish gastrointestinal tract.," Zebrafish, vol. 10, pp. 154–60, jun 2013.

[9] Y. Shi, Y. Zhang, F. Zhao, H. Ruan, H. Huang, L. Luo, and L. Li, "Acetylcholine serves as a derepressor in Loperamide-induced Opioid-Induced Bowel Dysfunction (OIBD) in zebrafish.," Scientific reports, vol. 4, p. 5602, 2014.

[10] A. Holmberg, C. Olsson, and G. W. Hennig, "TTX-sensitive and TTX-insensitive control of spontaneous gut motility in the developing zebrafish (Danio rerio) larvae.," The Journal of experimental biology, vol. 210, pp. 1084–91, mar 2007.

[11] A. Holmberg, T. Schwerte, B. Pelster, and S. Holmgren, "Ontogeny of the gut motility control system in zebrafish Danio rerio embryos and larvae.," The Journal of experimental biology, vol. 207, no. Pt 23, pp. 4085–4094, 2004.

[12] O. de Backer, B. Blanckaert, L. Leybaert, and R. a. Lefebvre, "A novel method for the evaluation of intestinal transit and contractility in mice using fluorescence imaging and spatiotemporal motility mapping.," Neurogastroenterology and motility : the official journal of the European Gastrointestinal Motility Society, vol. 20, pp. 700–7, jun 2008.

[13] H. a. Field, K. a. Kelley, L. Martell, a. M. Goldstein, and F. C. Serluca, "Analysis of gastrointestinal physiology using a novel intestinal transit assay in zebrafish.," Neurogastroenterology and motility : the official journal of the European Gastrointestinal Motility Society, vol. 21, pp. 304–12, mar 2009.

[14] T. a. Heanue, W. Boesmans, D. M. Bell, K. Kawakami, P. Vanden Berghe, and V. Pachnis, "A Novel Zebrafish ret Heterozygous Model of Hirschsprung Disease Identifies a Functional Role for mapk10 as a Modifier of Enteric Nervous System Phenotype Severity," PLOS Genetics, vol. 12, no. 11, p. e1006439, 2016.

[15] K. Sanders, "Regulation of smooth muscle excitation and contraction," Neurogastroenterology & Motility, vol. 20, no. s1, pp. 39–53, 2008.

[16] J. Wood and L. Johnson, "Physiology of the gastrointestinal tract," Raven, pp. 67–110, 1987. [17] S. Iino and K. Horiguchi, "Interstitial cells of cajal are involved in neurotransmission in the gastrointestinal tract.," Acta histochemica et cytochemica, vol. 39, no. 6, pp. 145–153, 2006.

[18] R. Baker, M. Taormina, M. Jemielita, and R. Parthasarathy, "A combined light sheet fluorescence and differential interference contrast microscope for live imaging of multicellular specimens," Journal of Microscopy, vol. 258, no. 2, pp. 2015.

[19] M. Jemielita, M. J. Taormina, A. Delaurier, C. B. Kimmel, and R. Parthasarathy, "Comparing phototoxicity during the development of a zebrafish craniofacial bone using confocal and light sheet fluorescence microscopy techniques.," Journal of biophotonics, vol. 6, pp. 920–8, dec 2013.

[20] P. J. Keller, A. D. Schmidt, J. Wittbrodt, and E. H. K. Stelzer, "Reconstruction of Zebrafish Early Light Sheet Microscopy," vol. 322, no. November, pp. 1065–1069, 2008.

[21] J. Huisken and D. Y. R. Stainier, "Selective plane illumination microscopy techniques in developmental biology.," Development (Cambridge, England), vol. 136, pp. 1963–75, jun 2009.

[22] P. a. Santi, "Light sheet fluorescence microscopy: a review.," The journal of histochemistry and cytochemistry : official journal of the Histochemistry Society, vol. 59, pp. 129–38, feb 2011.

[23] R. Tomer, K. Khairy, F. Amat, and P. J. Keller, "Quantitative high-speed imaging of entire developing embryos with simultaneous multiview light-sheet microscopy.," Nature methods, vol. 9, no. 7, pp. 755–63, 2012.

[24] U. Krzic, S. Gunther, T. E. Saunders, S. J. Streichan, and L. Hufnagel, "Multiview light-sheet microscope for rapid in toto imaging," Nature Methods, vol. 9, no. 7, pp. 730–733, 2012.

[25] B. Schmid, G. Shah, N. Scherf, M. Weber, K. Thierbach, C. P. Campos, I. Roeder, P. Aanstad, and J. Huisken, "High-speed panoramic light-sheet microscopy reveals global endodermal cell dynamics.," Nature communications, vol. 4, p. 2207, 2013.

[26] M. B. Ahrens, M. B. Orger, D. N. Robson, J. M. Li, and P. J. Keller, "Whole-brain functional imaging at cellular resolution using light-sheet microscopy," Nat Methods, vol. 10, no. 5, pp. 413–420, 2013.

[27] J. Swoger, M. Muzzopappa, H. L??pez Schier, and J. Sharpe, "4D retrospective lineage tracing using SPIM for zebrafish organogenesis studies," Journal of Biophotonics, vol. 4, no. 1-2, pp. 122–134, 2011.

[28] P. J. Keller and E. H. Stelzer, "Digital scanned laser light sheet fluorescence microscopy," Cold Spring Harbor Protocols, vol. 2010, no. 5, pp. pdb–top78, 2010.

[29] F. Cella Zanacchi, Z. Lavagnino, M. Perrone Donnorso, A. Del Bue, L. Furia, M. Faretta, and A. Diaspro, "Live-cell 3D super-resolution imaging in thick biological samples.," Nat Methods, vol. 8, no. 12, pp. 1047–9, 2011.

[30] M. Friedrich, Q. Gan, V. Ermolayev, and G. S. Harms, "STED-SPIM: Stimulated emission depletion improves sheet illumination microscopy resolution," Biophysical Journal, vol. 100, no. 8, pp. L43–L45, 2011.

[31] T. V. Truong, W. Supatto, D. S. Koos, J. M. Choi, and S. E. Fraser, "Deep and fast live imaging with two-photon scanned light-sheet microscopy.," Nature methods, vol. 8, pp. 757–60, sep 2011.

[32] M. J. Taormina, M. Jemielita, W. Zac Stephens, A. R. Burns, J. V. Troll, R. Parthasarathy, and K. Guillemin, "Investigating bacterial-animal symbioses with light sheet microscopy," Biological Bulletin, vol. 223, no. 1, pp. 7–20, 2012.

[33] R. Allen and G. David, "The zeiss-nomarski differential interference equipment for transmitted-light microscopy," Zeitschrift fur wissenschaftliche Mikroskopie und mikroskopische Technik, vol. 69, no. 4, pp. 193–221, 1969.

[34] M. Pluta, "Handbook: Advanced light microscopy. specialized methods vol. 2," 1989.

[35] S. H. Cody, S. D. Xiang, M. J. Layton, E. Handman, M. H. C. Lam, J. E. Layton, E. C. Nice, and J. K. Heath, "A simple method allowing DIC imaging in conjunction with confocal microscopy," Journal of Microscopy, vol. 217, no. 3, pp. 265–274, 2005.

[36] W. B. Amos, S. Reichelt, D. M. Cattermole, and J. Laufer, "Re-evaluation of differential phase contrast (DPC) in a scanning laser microscope using a split detector as an alternative to differential interference contrast (DIC) optics," Journal of Microscopy, vol. 210, no. 2, pp. 166–175, 2003.

[37] C. Preza, D. L. Snyder, and J. a. Conchello, "Theoretical development and experimental evaluation of imaging models for differential-interference-contrast microscopy.," Journal of the Optical Society of America. A, Optics, image science, and vision, vol. 16, pp. 2185–99, sep 1999.

[38] S. B. Mehta and C. J. R. Sheppard, "Partially coherent image formation in differential interference contrast (DIC) microscope.," Optics express, vol. 16, pp. 19462–79, nov 2008.

[39] S. B. Mehta and C. J. R. Sheppard, "Sample-less calibration of the differential interference contrast microscope.," Applied optics, vol. 49, pp. 2954–68, may 2010.

[40] V. Bormuth, J. Howard, and E. Sch¨affer, "LED illumination for video-enhanced DIC imaging of single microtubules.," Journal of microscopy, vol. 226, pp. 1–5, apr 2007.

[41] K. Dooley and L. I. Zon, "Zebrafish: a model system for the study of human disease.," Current opinion in genetics & development, vol. 10, no. 3, pp. 252–256, 2000.

[42] D. J. Grunwald and J. S. Eisen, "Headwaters of the zebrafish–emergence of a new model vertebrate," Nature reviews. Genetics, vol. 3, no. 9, p. 717, 2002.

[43] J. F. Rawls, M. A. Mahowald, A. L. Goodman, C. M. Trent, and J. I. Gordon, "In vivo imaging and genetic analysis link bacterial motility and symbiosis in the zebrafish gut," Proceedings of the National Academy of Sciences of the United States of America, vol. 104, no. 18, pp. 7622–7627, 2007.

[44] M. Jemielita, M. J. Taormina, A. R. Burns, J. S. Hampton, A. S. Rolig, K. Guillemin, and R. Parthasarathy, "Spatial and temporal features of the growth of a bacterial\nspecies colonizing the zebrafish gut," MBio, vol. 5, no. 6, pp. 1–8, 2014.

[45] I. Semova, J. D. Carten, J. Stombaugh, L. C. MacKey, R. Knight, S. A. Farber, and J. F. Rawls, "Microbiota regulate intestinal absorption and metabolism of fatty acids in the zebrafish," Cell Host and Microbe, vol. 12, no. 3, pp. 277–288, 2012.

[46] K. Milligan-Myhre, J. R. Charette, R. T. Phennicie, W. Z. Stephens, J. F. Rawls, K. Guillemin, and C. H. Kim, "Study of host–microbe interactions in zebrafish," Methods in cell biology, vol. 105, p. 87, 2011.

[47] R. Parthasarathy, "Rapid, accurate particle tracking by calculation of radial symmetry centers," Nature Methods, vol. 9, no. 7, pp. 724–726, 2012.

[48] L. L. McCarter, "Polar Flagellar Motility of the Vibrionaceae," Microbiology and Molecular Biology Reviews, vol. 65, no. 3, pp. 445–462, 2001.

[49] S. Renshaw and C. Loynes, "A transgenic zebrafish model of neutrophilic inflammation," Blood. . . , vol. 108, no. 13, pp. 3976–3978, 2006.

[50] J. Ganz, R. P. Baker, M. K. Hamilton, E. Melancon, P. Diba, J. S. Eisen, and R. Parthasarathy, "Image velocimetry and spectral analysis enable quantitative characterization of larval zebrafish gut motility," bioRxiv, 2017.

[51] E. Brosens, A. J. Burns, A. S. Brooks, I. Matera, S. Borrego, I. Ceccherini, P. K. Tam, M. M. Garć ıa-Barcel ́o, N. Thapar, M. A. Benninga, R. M. Hofstra, and M. M. Alves, "Genetics of enteric neuropathies," Developmental Biology, vol. 417, no. 2, pp. 198–208, 2016.

[52] A. M. Goldstein and N. Nagy, "A bird's eye view of enteric nervous system development: lessons from the avian embryo," Pediatr Res, vol. 64, no. 4, pp. 326–333, 2008.

[53] J. B. Furness, "The enteric nervous system," 2006.

[54] J. D. Huizinga and W. J. E. P. Lammers, "Gut peristalsis is governed by a multitude of cooperating mechanisms.," American journal of physiology. Gastrointestinal and liver physiology, vol. 296, no. 1, pp. G1–8, 2009.

[55] E. Deloose, P. Janssen, I. Depoortere, and J. Tack, "The migrating motor complex: control mechanisms and its role in health and disease," Nature Reviews Gastroenterology and Hepatology, vol. 9, no. 5, pp. 271–285, 2012.

[56] C. Olsson and S. Holmgren, "Autonomic control of gut motility: A comparative view," Autonomic Neuroscience: Basic and Clinical, vol. 165, no. 1, pp. 80–101, 2011.

[57] J. D. Wood, "Enteric nervous system: reflexes, pattern generators and motility," Current opinion in gastroenterology, vol. 24, no. 2, pp. 149–158, 2008.

[58] K. M. Sanders, S. M. Ward, and S. D. Koh, "Interstitial cells: regulators of smooth muscle function.," Physiological reviews, vol. 94, no. 3, pp. 859–907, 2014.

[59] J. B. Furness, B. P. Callaghan, L. R. Rivera, and H.-J. Cho, The Enteric Nervous System and Gastrointestinal Innervation: Integrated Local and Central Control, pp. 39–71. New York, NY: Springer New York, 2014.

[60] G. W. Hennig, M. Costa, B. N. Chen, and S. J. H. Brookes, "Quantitative analysis of peristalsis in the guinea-pig small intestine using spatio-temporal maps," Journal of Physiology, vol. 517, no. 2, pp. 575–590, 1999.

[61] P. W. Janssen and R. G. Lentle, "Spatiotemporal mapping techniques for quantifying gut motility," in New Advances in Gastrointestinal Motility Research, pp. 219–241, Springer, 2013.

[62] A. Holmberg, T. Schwerte, R. Fritsche, B. Pelster, and S. Holmgren, "Ontogeny of intestinal motility in correlation to neuronal development in zebrafish embryos and larvae," Journal of Fish Biology, vol. 63, pp. 318–331, aug 2003.

[63] J. Ganz, E. Melancon, and J. S. Eisen, Zebrafish as a model for understanding enteric nervous system interactions in the developing intestinal tract, vol. 134. Elsevier Ltd, 2016.

[64] X. Zhao and M. Pack, "Modeling intestinal disorders using zebrafish," Methods in Cell Biology, vol. 138, pp. 241–270, 2017.

[65] T. J. Wiles, M. Jemielita, R. P. Baker, B. H. Schlomann, S. L. Logan, J. Ganz, E. Melancon, J. S. Eisen, K. Guillemin, and R. Parthasarathy, "Host Gut Motility Promotes Competitive Exclusion within a Model Intestinal Microbiota," PLoS Biology, vol. 14, no. 7, pp. 1–24, 2016.

[66] C. E. Willert and M. Gharib, "Experiments in Fluids Digital particle image velocimetry," vol. 193, pp. 181–193, 1991.

[67] W. Thielicke and E. J. Stamhuis, "PIVlab Towards User-friendly, Affordable and Accurate Digital Particle Image Velocimetry in MATLAB," Journal of Open Research Software, vol. 2, 2014.

[68] J. Kuhlman and J. S. Eisen, "Genetic screen for mutations affecting development and function of the enteric nervous system," Developmental Dynamics, vol. 236, no. 1, pp. 118–127, 2007.

[69] L. Uyttebroek, I. Shepherd, P. Vanden Berghe, G. Hubens, J.-P. Timmermans, and L. Van Nassauw, "The zebrafish mutant lessen: an experimental model for congenital enteric neuropathies," Neurogastroenterology & Motility, vol. 28, no. 3, pp. 345–357, 2016.

[70] A. Holmberg, C. Olsson, and S. Holmgren, "The effects of endogenous and exogenous nitric oxide on gut motility in zebrafish Danio rerio embryos and larvae.," The Journal of experimental biology, vol. 209, no. Pt 13, pp. 2472–2479, 2006.

[71] A. S. Rolig, E. K. Mittge, J. Ganz, J. V. Troll, E. Melancon, T. J. Wiles, K. Alligood, W. Z. Stephens, J. S. Eisen, and K. Guillemin, "The enteric nervous system promotes intestinal health by constraining microbiota composition," PLoS Biology, vol. 15, no. 2, pp. 1–22, 2017.

[72] M. C. Lafave, G. K. Varshney, M. Vemulapalli, J. C. Mullikin, and S. M. Burgess, "A Defined Zebrafish Line for High-Throughput Genetics and Genomics: NHGRI-1," Genetics, vol. 198, no. 1, pp. 167–170, 2014.

[73] C. B. Kimmel, W. W. Ballard, S. R. Kimmel, B. Ullmann, and T. F. Schilling, "Stages of embryonic development of the zebrafish.," Developmental dynamics : an official publication of the American Association of Anatomists, vol. 203, pp. 253–310, jul 1995.

[74] T.-Y. Chang, C. Pardo-Martin, A. Allalou, C. Ẅahlby, and M. F. Yanik, "Fully automated cellular-resolution vertebrate screening platform with parallel animal processing.," Lab on a chip, vol. 12, pp. 711–6, mar 2012.

[75] E. J. Gualda, H. Pereira, T. Vale, M. F. Estrada, C. Brito, and N. Moreno, "SPIM-fluid: open source light-sheet based platform for high-throughput imaging," Biomedical Optics Express, vol. 6, no. 11, p. 4447, 2015.

[76] A. S. Rolig, R. Parthasarathy, A. R. Burns, B. J. Bohannan, and K. Guillemin, "Individual members of the microbiota disproportionately modulate host innate immune responses," Cell Host and Microbe, vol. 18, no. 5, pp. 613–620, 2015.

[77] S. Wolf, W. Supatto, G. Debrégeas, P. Mahou, S. G. Kruglik, J.-M. Sintes, E. Beaurepaire, and R. Candelier, "Whole-brain functional imaging with two-photon light-sheet microscopy," Nature Methods, vol. 12, no. 5, pp. 379–380, 2015.